



Nuno Miguel Gonçalves Pinela

Licenciado em Ciências da Engenharia de Micro e Nanotecnologias

Piezoresistive pressure sensor for application in e-skin devices

Dissertação para obtenção do Grau de Mestre em
Engenharia de Micro e Nanotecnologias

Orientador: Doutor Rui Alberto Garção Barreira do Nascimento
Igreja, Professor auxiliar, Faculdade de Ciências e
Tecnologia da Universidade Nova de Lisboa
Co-orientador: Doutor Hugo Manuel Brito Águas,
Professor auxiliar, Faculdade de Ciências e
Tecnologia da Universidade Nova de Lisboa

Júri

Presidente: Doutor Rodrigo Ferrão de Paiva Martins
Arguente: Doutor Carlos Jorge Mariano Miranda Dias
Vogal: Doutor Rui Alberto Garção Barreira do Nascimento Igreja



FACULDADE DE
CIÊNCIAS E TECNOLOGIA
UNIVERSIDADE NOVA DE LISBOA

Setembro, 2017

Piezoresistive pressure sensor for application in e-skin devices

Copyright © Nuno Miguel Gonçalves Pinela, Faculdade de Ciências e Tecnologia, Universidade NOVA de Lisboa.

A Faculdade de Ciências e Tecnologia e a Universidade NOVA de Lisboa têm o direito, perpétuo e sem limites geográficos, de arquivar e publicar esta dissertação através de exemplares impressos reproduzidos em papel ou de forma digital, ou por qualquer outro meio conhecido ou que venha a ser inventado, e de a divulgar através de repositórios científicos e de admitir a sua cópia e distribuição com objetivos educacionais ou de investigação, não comerciais, desde que seja dado crédito ao autor e editor.

*"Try not to become a man of success, but rather try to become a
man of value."
Albert Einstein*

Acknowledgements

I would like to acknowledge everyone who contributed for this master thesis to happen and to be concluded, starting from Professor Rodrigo Martins and Professor Elvira Fortunato, who have developed these two multidisciplinary research centers, which are CENIMAT|i3N and CEMOP, where I have spent my last nine months and where I found all the tools to surpass barriers and acquire knowledge. I would also like to show my acknowledgement to this great institution, FCT-UNL, where I find myself growing and evolving everyday, since the first day I joined it.

Secondly, I would like to express my gratitude to Professor Rui Igreja, for accepting and introducing me to this wide world of sensors. Furthermore, I would like to thank for the guidance and orientation in every single meeting. I am also grateful to Andreia, who has supported me and contributed significantly for this thesis. To Professor Hugo Águas, I also want to thank for the guidance.

Moreover, I want to thank CENIMAT|i3N members Alexandra Gonçalves, Sónia Pereira, Ana Carolina Marques, Ana Samouco, Beatriz Coelho, Ricardo Ferreira, Tiago Mateus, Rodrigo Santos, Pedro Alves, Daniela Gomes and Tomás Calmeiro, who have always provided me the help I needed, in terms of suggestions, logistics and technical support.

To all my friends from Open-Space, I want to give special thanks because in spite of our duty to complete this hard task of writing a master thesis, we managed to have fun and to help each others in one or another situation.

To my course friends who have been these last five years with me, João Afonso, Marco and Shiv. To my friend Tiago Gameiro, I would really like to express my gratitude, for the good times we have spent during these years. To my long-time friends Alexandre Ferrão, Gonçalo Félix and Duarte Pais, who have been an important support. Also, I want to thank to my girlfriend's family for the support.

I want to specially acknowledge all my family. To my grandparents for all the pride they put on me. To my parents Anabela and António, for conceding me this opportunity of education. I will be forever grateful, and will always praise on follow the principles I have been taught. To my brother Pedro, who has been a major pillar throughout the years. I also want to thank Noa for the unconditional love. To Mariana, who has made this walk alongside me, making it much easier. A few lines here would not be enough to express how thankful I am for all the love, support, motivation and for everything she is.

Abstract

In recent years, the advancement of science and technology tends to evolve towards the exploitation of electronic skin (e-skin) and functional prosthetic devices, enabling innovating applications in various fields such as biomedical systems, sports health-monitoring and healthcare. Owing to their significant role in health monitoring, pressure sensors come as essential components in the development of artificial systems that can mimic the impressive human skin. The development of such sensors comprises the search for flexible and stretchable materials suitable for implementation in robust devices that enable the integration of multiple sensing-functionalities. To quantitatively monitor pressure, these sensors use transduction methods based on piezoresistivity, capacity, piezoelectricity, and triboelectricity.

In this work, piezoresistive devices were chosen over others due to their ease in structure design and readout mechanism. The mechanism of such piezoresistive pressure sensor relies on the transduction of a pressure change into a change in resistance that, in this case derives from variations in the contact area.

In the approach presented in this work, a semi-sphere microstructuring patterning made by laser engraving on [hard-poly\(dimethylsiloxane\) \(h-PDMS\)](#) was introduced. [h-PDMS](#) works as a mold from which [standard-poly\(dimethylsiloxane\) \(s-PDMS\)](#) microstructured membranes with approximately 200 μm thickness are peeled off. Carbon-ink, working as active material, was deposited on top of the microstructured [s-PDMS](#) membranes. The fabrication of such pressure sensors based on organic membranes combines advantages such as the production in a low-cost and fast way, device flexibility, and tunability of the sensor's design. Moreover, sensitivities of $2.4 \times 10^{-1} \text{ kPa}^{-1}$ were reached for the sensors developed.

Keywords: Electronic skin, piezoresistivity, microstructures, semi-spheres, PDMS.

Nos últimos anos, o avanço da ciência e da tecnologia tende a evoluir para a exploração da pele eletrónica (e-skin) e próteses funcionais, possibilitando aplicações inovadoras em vários campos, nomeadamente sistemas biomédicos, saúde desportiva, e monitorização da saúde. Devido ao seu papel significativo na monitorização da saúde, os sensores de pressão são componentes essenciais no desenvolvimento de sistemas artificiais que conseguem imitar a impressionante pele humana. O desenvolvimento destes sensores requer a procura por materiais flexíveis e extensíveis adequados para implementação em dispositivos robustos que permitam a integração de múltiplas funcionalidades de detecção. Para monitorizar a pressão, estes sensores usam métodos de transdução baseados em piezoresistividade, capacidade, piezoelectricidade e triboelectricidade.

Neste trabalho, dispositivos piezoresistivos foram escolhidos em detrimento dos outros devido à sua fácil implementação e mecanismo de leitura. Este mecanismo consiste na transdução de uma diferença de pressão numa diferença de resistência que, neste caso, deriva de variações na área de contato.

Na nova abordagem apresentada neste trabalho, introduziu-se um método de microestruturação de semi-esferas baseado na gravação a laser em poli(dimetilsiloxano)-duro (h-PDMS). O h-PDMS funciona como um molde a partir do qual se retiram membranas microestruturadas de poli(dimetilsiloxano)-standard (s-PDMS) com aproximadamente 200 μm de espessura. O material ativo em cima do domínio microestruturado é tinta de carbono. A fabricação destes sensores de pressão com base em membranas orgânicas combina vantagens como a produção de forma rápida, fabricação de baixo custo, flexibilidade do dispositivo e flexibilidade na mudança do design do sensor. Para além disso, para estes sensores foram conseguidas sensibilidades de $2.4 \times 10^{-1} \text{ kPa}^{-1}$.

Palavras-chave: Pele electrónica, piezoresistividade, microestructuras, semi-esferas, PDMS.

Contents

List of Figures	xv
List of Tables	xvii
Acronyms	xix
Motivation and Objectives	xxi
1 Introduction	1
1.1 Electronic Skin	1
1.2 Pressure Sensor Fundamentals	1
1.3 Piezoresistive pressure sensor devices	3
1.3.1 Substrate Materials	4
1.3.2 Active Materials	5
2 Materials and Methods	7
2.1 Chemicals and Materials	7
2.2 Fabrication and laser engraving of PDMS molds	7
2.3 Fabrication of the piezoresistive pressure sensor devices	8
2.4 Morphological characterization of microstructured PDMS films	9
2.5 Characterization of carbon-coated membranes	9
2.6 Electrical characterization of devices	10
3 Results and Discussion	11
3.1 Patterning	11
3.2 Ink Study	18
3.2.1 Carbon-ink dilution study	18
3.2.2 Ink layers study	19
3.2.3 Electrical Characterization of carbon-coated membranes	20
3.2.4 Morphological Characterization of carbon-coated membranes	20
3.3 Homemade Pressure Applying System	22
3.4 Electrical Characterization of Devices	25
4 Conclusions and future perspectives	29
Bibliography	31
A Semi-sphere's dimensions measurements	37
B I-V tests	39
C Coated-PDMS microstructures measurements	41

CONTENTS

D Pressure applying system	43
E Sensor operation principle	47
F Resistance changes for different frequencies	49
G Estimated sensor price	51

List of Figures

1.1	Two main strategies to fabricate devices with improved stretchability	3
2.1	Schematic showing the principle steps of pressure sensors conception.	8
2.2	Photograph showing the bendability/flexibility of (a) one microstructured membrane that was peeled off from a h-PDMS mold. (b) the fabricated device	8
3.1	SEM images acquired from a top view of peeled membranes from molds made in s-PDMS in vector mode	12
3.2	Semi-Spheres height versus Laser Power	14
3.3	Real Diameter versus Designed Diameter	16
3.4	Real pitch versus Designed Pitch	16
3.5	Molds produced for fabrication of membranes.	17
3.6	Microscope acquired images of the fabricated molds.	17
3.7	Sheet resistance of smooth carbon-coated PMDS and PMMA-coated PDMS for four different carbon-ink dilutions in water.	18
3.8	Number of carbon coating layers study.	19
3.9	Block diagram representing the blocks constituting the system built.	22
3.10	Circuit design for the development of the system.	23
3.11	Picture representing the pressure applying system developed.	24
3.12	Pressure applied on piezoelectric sensor versus time.	25
3.13	Voltage sweep from -2 to 2 V proving the ohmic behaviour of two devices	26
3.14	Resistance changes in response to applied pressure over time	27
3.15	Resistance response to different pressures.	28
B.1	Voltage sweep from -2 to 2 V proving the ohmic behaviour of four membranes.	39
D.1	Schematic representation of the developed system.	44
D.2	Sketch in SketchUp of component 1 of the homemade system.	45
D.3	Sketch in SketchUp of components 2 and 3 of the homemade system.	45
D.4	Sketch in SketchUp of component 4 of the homemade system.	45
D.5	RC Low-Pass Filter with Op Amp Buffer.	46
E.1	Sensor operation principle based on resistance changes in responses to loading and unloading.	47
F.1	Resistance changes in response to an applied pressure	49

List of Tables

1.1	State of the Art of piezoresistive pressure sensors	4
3.1	Membranes peeled off from molds fabricated in s-PDMS using three different designs	11
3.2	Membranes peeled off from molds fabricated in h-PDMS using laser engraving in raster mode, power of 50 W, and a speed of 0.762 m/s.	13
3.3	Summary of height measurements of semi-spheres using different combinations of designed base diameters and laser powers.	14
3.4	SEM images acquired of microstructured PDMS films.	15
3.5	SEM images of microstructures produced on PDMS with carbon or PMMA + carbon coatings.	21
A.1	Semi-spheres real diameter and real pitch measured on horizontal and vertical directions	37
C.1	Measurements of dimensions of the fabricated microstructures with carbon coating and with carbon coating with PMMA.	41
G.1	Estimated sensor price regarding materials costs	51

Acronyms

CNTs	carbon nanotubes.
h-PDMS	hard-poly(dimethylsiloxane).
LCD	liquid crystal display.
LOD	limit of detection.
PDMS	poly(dimethylsiloxane).
PEDOT:PSS	poly(3,4-ethylenedioxythiophene) polystyrene sulfonate.
PEN	polyethylene.
PI	polyimide.
PMMA	poly(methyl methacrylate).
PVDF	poly(vinylidene) difluoride.
PZT	lead zirconate titanate.
SEM	scanning electron microscope.
s-PDMS	standard-poly(dimethylsiloxane).

Motivation and Objectives

Nowadays, the pursuit for information-sensing inspired by human skin has been motivated by the possibility of application on functional health monitoring systems and on robotic systems. Therefore, in order to achieve this, thin film pressure sensors are being widely exploited.

Furthermore, efforts have been made towards the fabrication of thin film sensors in a non-clean room environment, which would considerably lower the device cost. Thus, the main goal of this work is to design, fabricate and develop low-cost, flexible pressure sensors based on the piezoresistive effect, which could be easily adapted and conformed to different surfaces, using microstructured substrates.

Large scale production greatly benefits from low manufacturing costs in flexible pressure sensors, and the simplification of the device's structure and manufacture is also desirable. These piezoresistivity-based devices allow an easy readout mechanism, as well as a simple structure design, which in turn will allow an easy device optimization. Moreover, through the use of the perfect combination of materials one expects to produce each sensor for approximately 0.351 € (materials costs).

Finally, the fabricated materials will be extensively characterized, both morphologically and electrically, as to compare different designs, with the primary goal of developing a sensor with the best sensitivity possible.

Introduction

1.1 Electronic Skin

Human skin is an outstanding organ, being our interface with the surrounding world and allowing us to perceive mechanical stimuli such as pressure, shapes and textures [1]. This sense of information is only achievable because human skin comprises mechanoreceptors that receive a mechanical stimulus which is then transduced into a biological response [2]. Nowadays, inspired by this illusory simplicity of nature, efforts are being made to develop skin-inspired electronic devices. The pursuit for these e-skin devices is motivated by the possibility of application on functional prosthetic devices [3], humanoid robotics [4] and human health monitoring, where it could play a key role [5, 6]. Therefore, accurate quantitative monitoring requires an effective transduction where transduction mechanisms such as piezoresistivity [7–9], capacitance [10–12], piezoelectricity [13–15], and triboelectricity [16–18] are being widely exploited to develop different types of pressure sensors.

1.2 Pressure Sensor Fundamentals

Firstly, for a better comprehension of pressure distributions, pressures such as human touch, object manipulation, and human body circulation are considered to be in the low pressure (<10 kPa) and medium-pressure (10-100 kPa) regimes [12]. Secondly, and given that a pressure sensor transduces a mechanical pressure into an electrical signal an outline of some noteworthy key parameters that include sensitivity, **limit of detection (LOD)**, linearity, response time and stability is presented. Among these, sensitivity, which is defined by the ratio between the variation of the quantitative output signal and variation of the applied pressure, is one of the most important parameters because it defines the accuracy and effectiveness of the measurement [19]. Sensitivity is defined as

$$S = \frac{\left(\frac{\Delta R}{R_0}\right)}{\Delta P} \quad (1.1)$$

Where P denotes the applied pressure and $\Delta R/R_0$ is the relative resistance change of the sensor.

LOD represents the lowest quantity of pressure that can be distinguishable. Lowering the **LOD** of a pressure sensor represents an improvement on lower pressure detection which is a requirement in lower pressure regimes [20].

Another relevant parameter is linearity, which is a classification expressed as percentage of the deviation of the sensor's output curve from a specified straight line over a

certain pressure range [20]. Hence, one desires to have pressure sensors with broad linear ranges, which simplifies the conversion of mechanical pressure into electrical output.

Response time can be defined as the time required for a pressure sensor output to go from its previous state to a final stable value [20]. This parameter is especially important in dynamic real-time pressure sensing devices, when producing real-time monitoring systems or instant-response displays.

Furthermore, to accurately measure the magnitude of a pressure stimulus, the most relevant transduction methods are piezoelectricity, capacitance, and piezoresistivity .

Piezoelectricity, which is the ability (quantified by the piezoelectric strain constant d_{33}) of a material to generate electrical charges in response to the occurrence of electrical dipole moments due to applied mechanical stresses. This property of crystals and certain ceramics is good for development of low-power-consumption or self-powered sensing devices [21]. Moreover, the piezoelectric element of the device can be combined with transistors to improve sensitivity [13]. The development of piezoelectric pressure sensors has been receiving lots of attention due to their fast response speed and self-powered operation. The piezoelectric materials most used for this application include poly(vinylidene) difluoride (PVDF) and its copolymers, lead zirconate titanate (PZT) [13], and Zinc Oxide (ZnO) [22].

Capacitive sensor transduction consists of a change in capacitance caused by the deflection of the plate when an external stimulus is applied. As dielectric constant (permittivity) of the medium between the plates is a constant, the external stimulus, either an applied pressure or shear force, usually represents a change in area or in the distance between the plates, respectively [1].

Capacitive sensors offer advantages such as high sensitivity, but the main advantage of this types of sensors is the simplicity of their governing equation, which allows a direct analysis and a simple device design [23]. These sensors have also demonstrated the characteristic of high strain sensitivity for detection of a static force with low-power consumption [24]. However, once capacitance is proportional to the area, a reduction in the size of these devices for miniaturization means a reduction of the capacitance and the signal-to-noise ratio [25]. Additionally, capacitive sensors are vulnerable to external interferences [26].

The other transduction method commonly used is based on piezoresistive effect. Piezoresistive sensors have been widely investigated due to their simple structure and readout mechanism [27]. These sensors transduce a force variation into changes in resistance of a device that is detected by an electrical measuring system. The resistance variation derives most commonly from changes in: the geometry of the sensing element; the contact resistance (R_C) and the resistivity of a composite due to changes in separation between particles. Usually, for these type of sensors, when the resistivity of the material is constant, a change in resistance derives from changes in the geometry of the sensing element.

For conductive materials, the mechanism relies on changes in the R_C between both materials. A R_C change caused by change in contact area between two conductors is

proportional to the square root of the force, which is an advantage as it provides high sensitivity at lower pressures as well as it expands the usable range [1]. For conductive elastic composites, piezoresistance depends on the morphology, composition, and strain range of the system, and the mechanism relies on changes in conductive path. Furthermore, piezoresistive sensors exhibit a fast response speed [1]. However, piezoresistivity-based sensors usually show undesirable drift and hysteresis [28].

As seen, the presented transduction methods provide different sensing capabilities which allows systems to integrate multifunctional sensors. For example, piezoresistive are usually used to reliably measure large strains [29], capacitive devices to sense normal forces and piezoelectric devices to measure vibrations [1].

1.3 Piezoresistive pressure sensor devices

Being human skin considered as a performance benchmark for the development of e-skin, some considerations need to be followed to grant this electrical material the mechanical properties of human skin, such as stretchability, flexibility, and low Young's modulus [1]. To fulfil these considerations, the design and fabrication of the device are critical. An important parameter is regarding device's stretchability and there are two main strategies used to improve it [30]. The first method (Figure 1.1a) uses a thin conductive material bonded to an elastic substrate, such as poly(dimethylsiloxane) (PDMS) [10]. The second method (Figure 1.1b) is based on the fabrication of devices by mixing conductive materials into an elastomeric matrix [31].

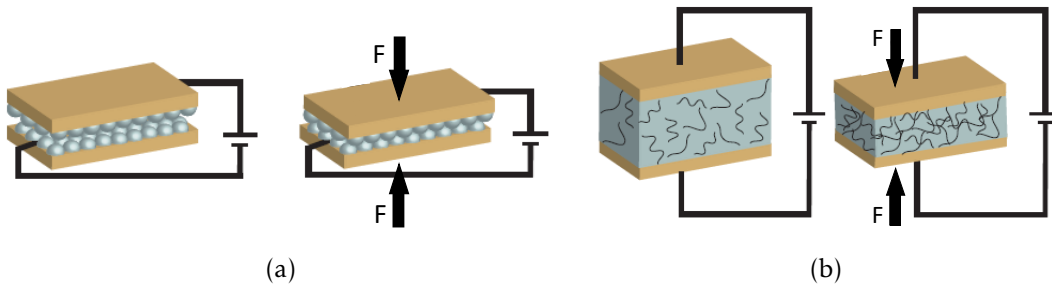


Figure 1.1: (a) Thin conductive material bounded to a micro-structured elastomer. (b) Mixture of a conductive material on an elastomeric matrix.

Another important parameter in pressure sensors design is the contact area, which can be increased by constructing various device geometries, for example through the materials microstructuration. Creating the desired geometry requires techniques such as lithography [32], coating [33], and micro-channel molding and filling [34]. This concept has shown to be an ideal candidate for e-skin applications [8, 12]. For this reason, and to be able to meet the needs stated above, the materials choice is crucial for the development of flexible pressure sensors and herein, an outline of substrate and active materials for piezoresistive pressure sensors is presented. Table 1.1 summarizes piezoresistive pressure sensors developed over the recent years as well as their performance parameters, to

understand the trend in piezoresistive pressure sensor development.

Table 1.1: State of the Art of piezoresistive pressure sensors. Abbreviations used in this table: Carbon Nanotubes (CNTs), Gold (Au), Gold Nanowires (AuNWs), Limit of Detection (LOD), Not Available (NA), Platinum (Pt), Poly(3,4-ethylenedioxythiophene) Polystyrene Sulfonate (PEDOT:PSS), Polydimethylsiloxane (PDMS), Polyurethane Dispersion (PUD), Single-walled Carbon Nanotubes (SWNTs), Zinc Oxide (ZnO).

Materials	Sensitivity (kPa^{-1})	(LOD) (Pa)	Operating Voltage (V)	Response time (ms)
[7] Pt-coated Nanohairs	NA	5	NA	50
[9] AuNWs coated tissue	1.14	13	1.5	<17
[27] Polypyrrole	133.1	0.8	NA	47
[35] PDMS/SWNTs	1.8	0.6	2	<10
[36] PDMS/PEDOT:PSS/PUD	10.3	23	0.2	200
[37] PDMS/Graphene	8.5	1	1	40
[38] PEDOT:PSS/ZnO nanorods	0.00617	NA	3	30
[39] Graphene	0.034	0.3	NA	40
[40] Au-coated polymer sponge	-0.31	<10	NA	<10
[8] PDMS/CNT mixture	-15.1	0.2	10	40

1.3.1 Substrate Materials

An e-skin pressure sensor requires flexible and stretchable substrates such as PDMS [41], polyimide (PI) [42], and polyethylene (PEN) [43]. PDMS is a silicon-based organic polymer that, among other applications, has been widely used in microfluidic chip fabrication [44]. PDMS films are currently the flexible substrates most used to integrate sensitive materials for the fabrication of e-skin and other flexible electronic applications. This fact is due to its commercial availability and well-researched properties, namely excellent elasticity, stability over a wide range of temperatures, conformability, transparency, ability to define adhesive regions for surface bonding with other materials through exposure to UV/O₂ irradiation [1], and biocompatibility, derived from its impermeability to water, nontoxicity to cells, and permeability to gases [35, 45]. One can realize that from the year 2014 on, the tendency was to fabricate microstructured PDMS-based sensors. The presented sensors comprising PDMS as substrate material show values of sensitivities in good agreement with each others and all above 1 kPa^{-1} .

Another flexible polymer is PI, which shows excellent stability and withstands large temperature ranges, given that this material has a small linear thermal expansion coefficient [42]. In literature, other flexible pressure sensors on PI substrates were developed, proving the stability of this polymer and the possibility of reaching a very thin thickness, allowing small radial bending [46]. According to literature, some other less conventional materials are used as substrate such as elastomeric fibers [47] and textiles [48].

1.3.2 Active Materials

Active materials play the most important role on pressure sensor design, as these are the components responsible for granting the device its transduction properties. The most commonly reported active materials are either conductive materials or elastomer conductive composites.

Conductive materials to be used in e-skins should be low cost, present a long-time endurance, and have a good adherence on substrates. In the search for these important characteristics, conductive inks such as silver ink come as particularly attractive materials for these type of e-skin sensors as they provide the stated and also show high conductivity, while allowing great stretchability and elasticity [49]. Another example of material is graphene which is a monoatomic thin carbon film with high conductivity [50]. This material seems to be suitable to act as an active material in pressure sensors due to its mechanical and electrical properties [50].

Conductive fillers such as [carbon nanotubes \(CNTs\)](#), metal particles, conductive nanotubes and nanowires of other materials besides carbon [9], and conductive polymers such as [poly\(3,4-ethylenedioxythiophene\) polystyrene sulfonate \(PEDOT:PSS\)](#) [36] are commonly used in elastomeric matrixes of [PDMS](#), sponge and other porous materials. To obtain these type of sensors, elastomers and conductive materials are mixed using appropriate methods and a "trade-off" between mechanical elasticity and electrical conductivity is a challenge because increasing conductivity is commonly only achievable by increasing the amount of the conductive filler, which means a decrease in elasticity. [CNTs](#) are the conductive fillers most commonly used due to their high conductivity and large anisotropy, as well as chemical stability [51]. [CNTs](#) in polymer matrixes have some disadvantages, as well, such as the different amount of impurities and structural defects resultant from preparations of [CNTs](#), which means that it is very difficult to produce [CNTs](#) with controlled reproducibility. Another challenge is the efficient translation of performance of a single nanotube into the performance of the system composed by the elastomer and the conductive fillers [52]. Other methods include the application of metal/metal-coated nanowires comprising a sensitivity of about 1 kPa^{-1} as shown on Table 1.1.

In this work the defining feature of the piezoresistive sensors was the design of the micro-structured domain on each membrane. Microstructuring the membranes results in an increase of the contact area, which affects the contact resistance, hence increasing the $R_{\text{OFF}}/R_{\text{ON}}$ ratio [8]. Herein, and inspired by the epidermal-dermal interlocked microstructures in human skin, semi-sphere designs were explored to amplify pressure signals, as shown on (Figure 1.1a). Furthermore, semi-spheres were chosen over other geometric shapes such as cones, cylinders or square pillars due to their easy fabrication process. On top of semi-spheres, carbon-ink played the role of active material of the device, conceding it its electrical properties.

Materials and Methods

2.1 Chemicals and Materials

PDMS elastomer and curing agent (Sylgard 184) - Dow Corning. poly(methyl methacrylate) (PMMA) (MW approximately 120,000) and trichloro(1H, 1H, 2H, 2H-perfluorooctyl)silane (97%) - Aldrich. Toluene (99.99%) - Fisher Scientific. Highly conductive water-based carbon coating (PE-C-808) and water-based silver conductive ink (PE-WB-1078) - Conductive Compounds.

2.2 Fabrication and laser engraving of PDMS molds

Herein, molds made of h-PDMS were used. The higher Young's modulus of h-PDMS is important to not only achieve a high fidelity between patterns but also to easily peel off standard PDMS membranes, with lower Young's modulus, from the mold [53]. Due to their lower Young's modulus, the peeled off PDMS membranes are designated s-PDMS. h-PDMS molds were fabricated by mixing PDMS curing agent to PDMS elastomer in a 1:5 w/w ratio. The mixture was then degassed in vacuum until all air bubbles had burst, and it was then dropped into a Petri dish. The Petri dish containing PDMS was posteriorly cured for about 1 hour at 70 °C.

Molds were microstructured by generating micro-cavities on the surface of 5-mm-thick h-PDMS sheets using a laser engraving machine (VLS3.50, 50 W, Universal Laser System, USA) with a carbon dioxide laser beam. This machine has a focus length of lens of 2.0 in. and the diameter of focal spot is 127 μm . Additionally, the laser engraving machine allows engraving in two different modes: vector and raster. In raster mode, the laser beam works in a straight line, etching each line at a time. On the contrary, when working in vector mode, the laser beam acts as an inkjet printer, printing the shape approximately as it is. The micro-cavities can be achieved by melting certain spots and what defines the aspect of the cavity is the power and duration of the laser beam on the spot, which is controlled by computer, as well as their initial design. The desired patterns to be engraved were previously designed in Adobe Illustrator (2015.0.0) and exported as CAD files. These patterns consist in replicating the same geometric figure the same times over rows and columns performing a window with 2 x 2 cm^2 .

After fabricating these molds, they were cleaned in an ultrasonic bath for 10 min in isopropanol alcohol, followed by a rinsing in MilliQ water. In order to easily peel off PDMS films from the engraved molds, these molds were placed in a desiccator for 30 min with 1 drop of trichloro(1H, 1H, 2H, 2H-perfluorooctyl)silane. This treatment provides the PDMS an hydrophobic layer of trichloro(1H, 1H, 2H, 2H-perfluorooctyl)silane, allowing

an easy peeling.

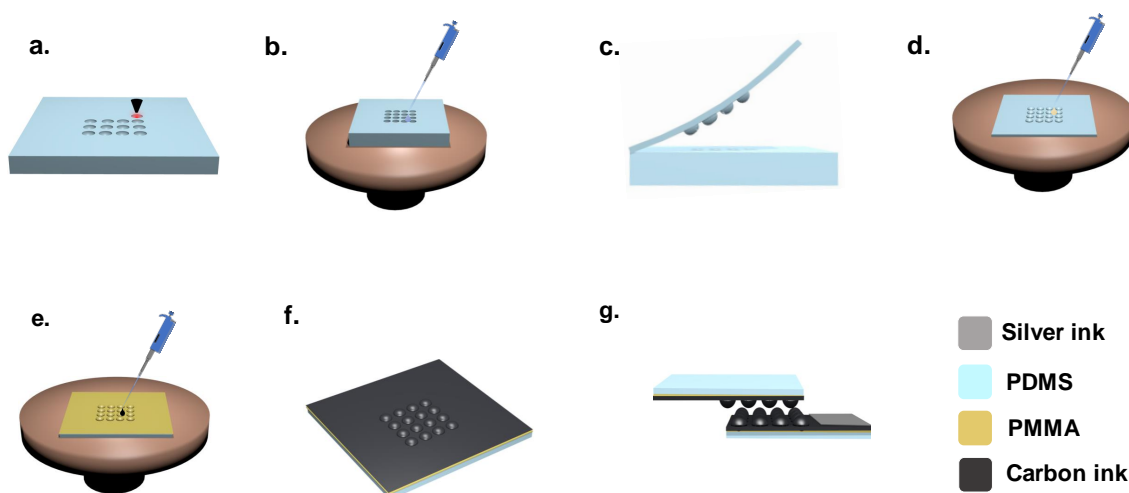


Figure 2.1: Schematic showing the main steps of pressure sensors conception. (a) h-PDMS mold (5 cm x 5 cm) being laser engraved with semi-sphere cavities. (b) s-PDMS spin-coating over the previously made h-PDMS mold. (c) Peeling off the flexible and already cured s-PDMS membrane from the h-PDMS mold containing the microstructures. (d) PMMA spin-coating on PDMS membrane. (e) Carbon-ink spin coating on the PMMA-coated PDMS membrane. (f) Carbon-ink coating on the membrane after curing. (g) Representation of the fabricated device by layers, with a silver-ink stripe on the smooth edge of each micro-structured PDMS film. Note that none of the steps are at scale.

2.3 Fabrication of the piezoresistive pressure sensor devices

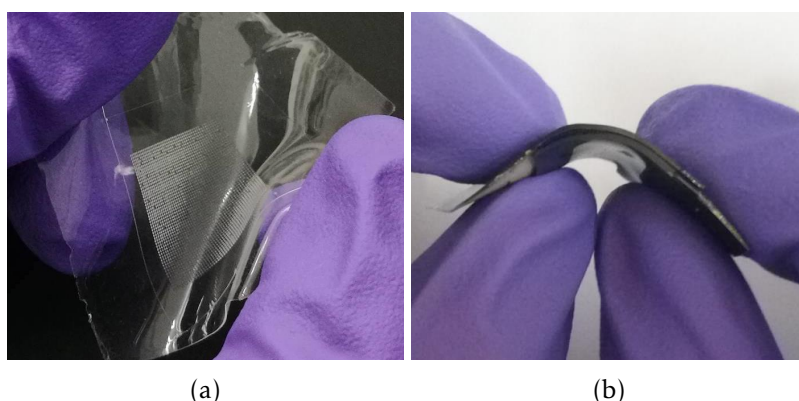


Figure 2.2: Photograph showing the bendability/flexibility of (a) one microstructured membrane that was peeled off from a h-PDMS mold. (b) the fabricated device

For the fabrication of the microstructured s-PDMS films, PDMS was prepared in a ratio of 1:10 w/w of curing agent to elastomer and subsequently degassed in vacuum until all air bubbles had burst. PDMS was posteriorly spin-coated at 250 rpm for 90 s onto each engraved mold in quantities of 1.5 mL, ensuring the whole 5 cm x 5 cm of mold were

uniformly covered. This process was followed by another degassing process performed for 30 min, granting the absence of bubbles in the curing process and ensuring the high fidelity between PDMS films and PDMS molds. The curing process occurred for 30 min at 85 °C in an Infrared IC Heater (T-962 Eco-Worthy). After curing, PDMS membranes were easily peeled off as shown on Figure 2.1, due to the silane treatment previously done on molds surface. Figure 2.2a shows a peeled off PDMS membrane containing the designed microstructured domain. PDMS membranes were then spin-coated at 1000 rpm for 20 s with highly conductive water-based carbon coating (PE-C-808), which plays the role of conductive material on the device. This carbon-ink coating was preceded by an O₂ plasma treatment (37.5 W for 1 min with an O₂ pressure of 0.3 mbar), which modifies PDMS surface with hydroxyl groups and makes it hydrophilic, facilitating adhesion of carbon ink on PDMS. Curing the carbon ink occurred for 30 min at 85 °C, and the result is shown on Figure 2.1.

To fabricate piezoresistive devices, carbon-ink-coated-membranes were then cut into the desired size (3 cm x 2 cm) and two membranes of the same pattern were sandwiched ensuring both micro-structured domains were centred with each other. Both membranes were finally sealed with 4 drops of PDMS in each corner. To ensure the good stability of the electrodes and to improve their conductivity, lines of water-based silver conductive ink (PE-WB-1078) were deposited on the edges of each film as shown on Figure 2.1. These lines were then cured at 145 °C for 120 s. Some experiments in this work use PMMA as a coating between PDMS and carbon-ink layer. PMMA (10 wt% in toluene) coating was also preceded by an O₂ plasma treatment (37.5 W for 1 min with an O₂ pressure of 0.3 mbar) and it was spin-coated onto the PDMS surface at 1000 rpm for 60 s. Thermal curing of PMMA films occurred in vacuum for 1 h at 140 °C.

2.4 Morphological characterization of microstructured PDMS films

Microstructured PDMS films peeled from each mold were then coated with a gold/palladium (Au/Pd) layer of 15 nm to 20 nm thickness in a turbo-pumped sputter coater (Quorum Q150T ES). Then, images of the films were acquired with a tabletop scanning electron microscope (SEM) (Hitachi TM3030Plus) in a standard observation mode at 15 kV using the software Hitachi TM3030Plus (01-04-02).

2.5 Characterization of carbon-coated membranes

To measure sheet resistance of membranes, Keithley 2000 Multimeter was used in a simple 2-wire configuration (as the resistance is expected to be large enough). The device directly displays the sheet resistance corresponding to a 2 cm × 2 cm square of carbon, placed between the silver electrodes previously defined. Furthermore, thickness of carbon

coating layers was measured in a profilometer (Ambios XP-Plus 200 Stylus) for one to five stacked layer depositions, using a tracking force of 0.5 mg and a scanning speed of 0.20 mm/sec. I-V curves were acquired using Keithley 2000 Multimeter connected to each silver-ink electrode of the membrane and a voltage sweep from -2 V to 2 V, in steps of 0.5 V, was applied. The output signal corresponds to current flowing through the 2 cm x 2 cm microstructured domain.

2.6 Electrical characterization of devices

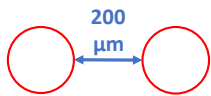

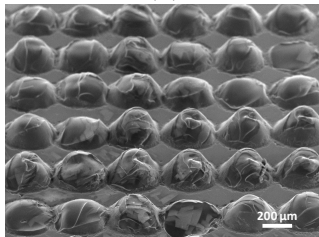
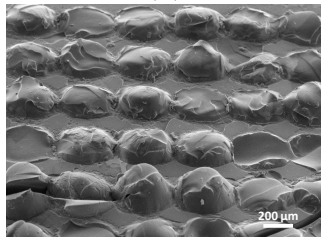
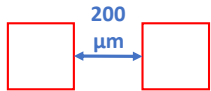

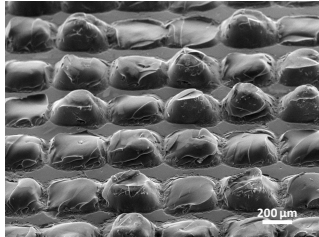
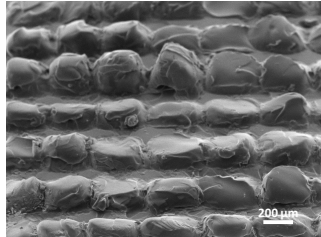
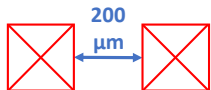
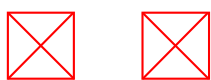
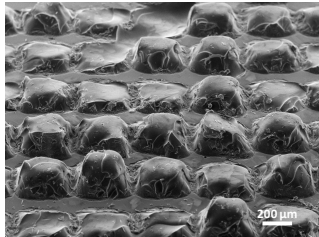
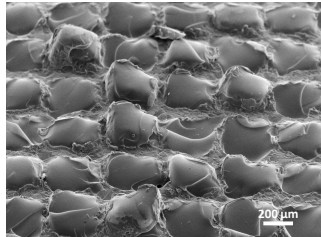
For quantitative analyses, output signals from a mechanical stimulus were acquired by recording changes in electrical resistance as a function of applied pressure using a home-made system developed on the scope of this work (as described in Section 3.3), capable of applying different pressure values. Additionally, I-V curves of the devices were acquired using the same method as for membranes, to test for ohmic-like behaviour.

Results and Discussion

3.1 Patterning

The microstructured domain shape optimization to reach semi-sphere-like structures went through several steps such as exploitation in PDMS molds fabrication, laser engraving parameters, and shape design in software.

Table 3.1: Membranes peeled off from molds fabricated in standard-PDMS using a speed of 0.254 m/s and laser power of 12.5 W for images (a)(c)(e) or laser power of 25 W for images (b)(d)(f), all with laser engraving in vector mode and for the three different designs previously mentioned. (a) and (b) Microstructures resultant from aligned circles with with both a diameter and a circles distance of 200 μm . (c) and (d) Microstructures resultant from aligned squares of 200 μm x 200 μm with a distance between squares of 200 μm . (e) and (f) Microstructures resultant from aliigned squares of 200 μm x 200 μm with two diagonals and a distance between squares of 200 μm . Abbreviations used in this table: Power (P), soft-Polydimethylsiloxane (s-PDMS), Speed (S).

Vector Mode s-PDMS	P = 12.5 W, S = 0.254 m/s	P = 25 W, S = 0.254 m/s
 	<p>(a)</p> 	<p>(b)</p> 
 	<p>(c)</p> 	<p>(d)</p> 
 	<p>(e)</p> 	<p>(f)</p> 

Firstly, tests over shape design in software were performed to choose the perfect design to achieve the desired form on laser engraving. To do so, three different shapes were studied: circles, squares, and squares with two diagonals. The circles had a diameter of $200\ \mu\text{m}$, the squares were $200\ \mu\text{m} \times 200\ \mu\text{m}$, and the pitch between each feature was fixed at $200\ \mu\text{m}$. These designs were engraved in vector mode in s-PDMS films in two different batches – the first with a laser power of $12.5\ \text{W}$ and a speed of $0.254\ \text{m/s}$ and the second with a laser power and speed of $25\ \text{W}$ and $0.254\ \text{m/s}$, respectively. Table 3.1 shows tilted images (45°) acquired from the membranes peeled off from molds. Molds engraved with circles clearly show a much more semi-sphere like structure, whereas the others stay more faithful to their squared designs. All six examples show some irregularities in the microstructures due to the difficult in peeling off the membranes from the mold made of the same material. Additionally, given that molds engraving is done in a material that melts very easily, the engraved cavities do not melt in a homogeneous way, and so the PDMS membranes that are peeled off from these molds get the negative pattern of those irregularities.

Membranes peeled off from the mold engraved with higher power present features that are more irregular, possibly due to the over-melting of PDMS during laser engraving. Therefore, molds engraved with a power of $12.5\ \text{W}$ and a speed of $0.254\ \text{m/s}$ appear to be preferred candidates for ideal semi-sphere molds.

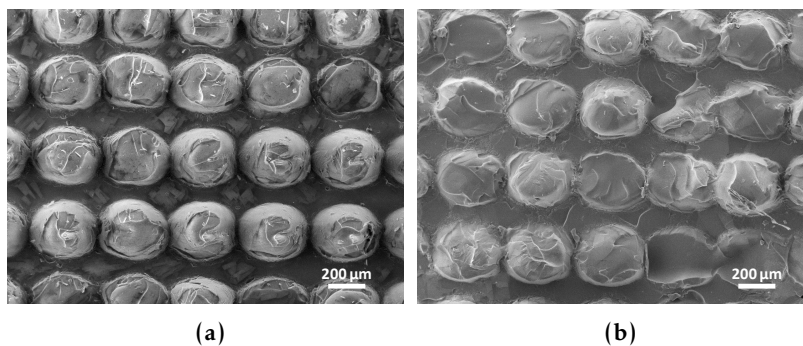


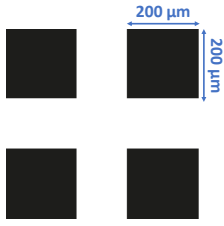
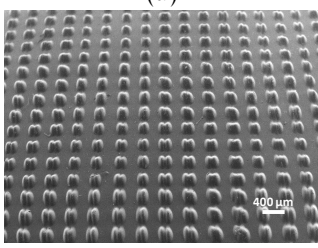
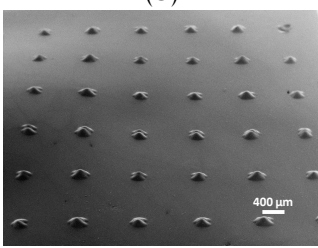
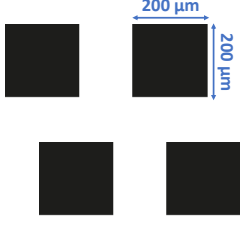
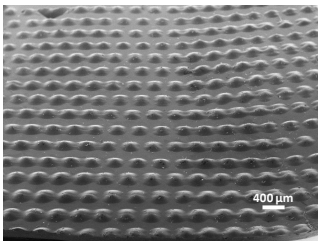
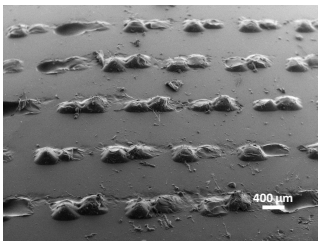
Figure 3.1: SEM images acquired from a top view of peeled membranes from molds made in s-PDMS in vector mode using a laser speed of $0.254\ \text{m/s}$ and a laser power of (a) $12.5\ \text{W}$ and (b) $25\ \text{W}$.

A top view of the semi-sphere like features from the achieved membranes was also captured, as shown on Figure 3.1. Such figure confirms a good fidelity to the design in terms of shape, but highlights differences in terms of pitch over the horizontal and vertical engraving directions. This discrepancy results from the fact that the laser has a better resolution on the vertical direction than on the horizontal direction as further examined in this section. Figure 3.1 also shows that the pitch ($200\ \mu\text{m}$) is close to the laser beam resolution ($127\ \mu\text{m}$) as semi-spheres in horizontal direction are almost touching their horizontal neighbour semi-spheres. This represents a limit in design's pitch (for these ranges of laser power), as a pitch lower than the one tested ($200\ \mu\text{m}$) would lead to

an over-melting of cavities on PDMS mold, resulting in distinct features than the ones designed.

Meanwhile, tests on h-PDMS were also performed to evaluate the combination of raster mode engraving on molds made of h-PDMS. The designs tested for this engraving mode had to be changed because raster mode engraves the material in a different way when compared to vector mode. Also, one expected that a design based on circles would give rise to cavities with the shape of inverted cones instead of inverted semi-spheres. Therefore, the patterns designed for this study were squares of $200\ \mu\text{m} \times 200\ \mu\text{m}$ with a pitch of $300\ \mu\text{m}$ or $1000\ \mu\text{m}$. Laser engraving parameters were fixed at a speed of $0.762\ \text{m/s}$ and power of $50\ \text{W}$. From patterns shown on Table 3.2 one can observe the formation of 3D structures far from being semi-spheres. For instance, in the image for the aligned pattern with the pitch = $300\ \mu\text{m}$, straight lines engraved by the laser beam are perfectly distinguishable, which confirms that raster mode is not suitable for regular semi-sphere microstructuring.

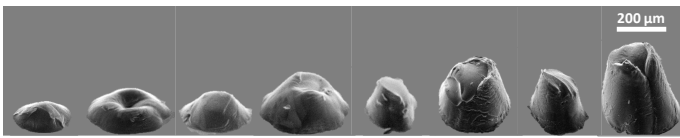
Table 3.2: Membranes peeled off from molds fabricated in h-PDMS using laser engraving in raster mode, power of $50\ \text{W}$, and a speed of $0.762\ \text{m/s}$. (a) Microstructures resultant from aligned squares of $200\ \mu\text{m} \times 200\ \mu\text{m}$ with a distance between squares of $300\ \mu\text{m}$. (b) Microstructures resultant from aligned squares of $200\ \mu\text{m} \times 200\ \mu\text{m}$ with a distance between squares of $1000\ \mu\text{m}$. (c) Microstructures resultant from misaligned squares of $200\ \mu\text{m} \times 200\ \mu\text{m}$ with a distance between squares of $300\ \mu\text{m}$. (d) Microstructures resultant from misaligned squares of $200\ \mu\text{m} \times 200\ \mu\text{m}$ with a distance between squares of $1000\ \mu\text{m}$.

Raster Mode h-PDMS	Pattern	Pitch = $300\ \mu\text{m}$	Pitch = $1000\ \mu\text{m}$
Aligned			
		(a)	(b)
Misaligned			
		(c)	(d)

Once the design and the laser engraving mode for microstructuring semi-spheres were chosen, the optimization process demanded a choice of the mold material. As seen before,

membranes peeled off from *s*-PDMS molds were usually difficult to peel and showed irregularities on their structure. Therefore, experiments in vector mode on *h*-PDMS were also performed to appraise this combination comprising circle patterns. Herein, to investigate the effect of laser power on engraving microcavities, molds were engraved using laser power of 25 W, 12.5 W, 7.5 W, and 2.5 W whereas the speed was fixed at 0.254 m/s for all patterns. The reason to maintain laser speed at a high value is due to the fact that the higher the laser speed, the shorter is the working time of laser on PDMS and, consequently, the less high and sharp the structures will be. Table 3.3 and Figure 3.2 present results from molds fabricated using laser vector mode on *h*-PDMS with circles, where one observes that the higher the laser power, the higher the microstructures are. In this specific study, a 45 % increase in laser power gives rise to structures with a height five times bigger.

Table 3.3: Summary of height measurements of semi-spheres using different combinations of designed base diameters and laser powers.



Height (μm)	60	80	112	151	180	206	232	320
Diameter (μm)	100	200	100	200	100	200	100	200
Laser Power (W)	2.5	2.5	7.5	7.5	12.5	12.5	25	25

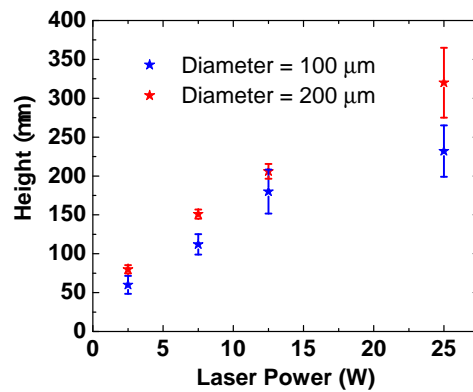
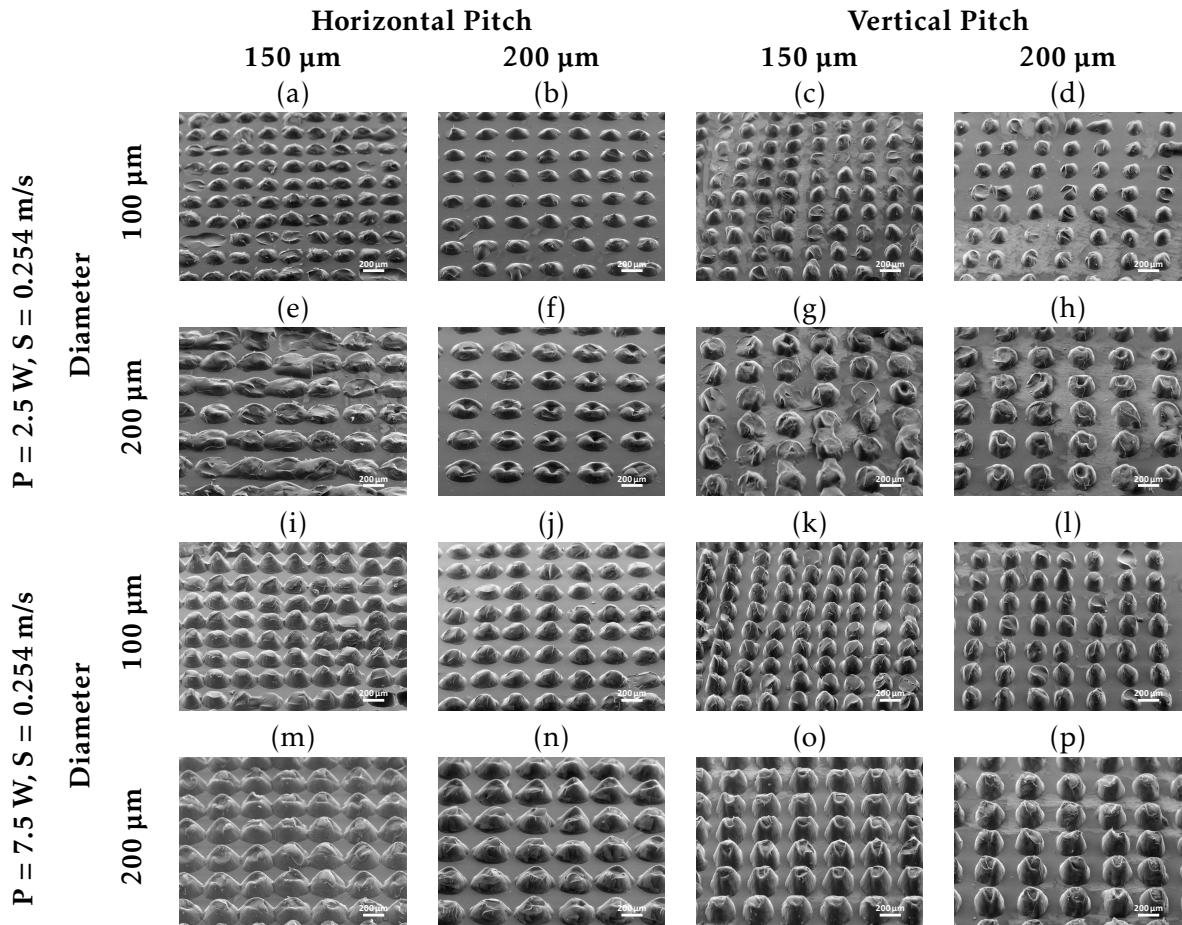


Figure 3.2: Semi-spheres height measured from SEM images versus laser power used to engrave the molds from where the resultant structures were peeled off. Values presented correspond to average values \pm standard deviation of a minimum of 15 measurements.

A relation between diameter and height is also observable, once the higher the designed diameter, the higher the semi-sphere height is. This results from the fact that engraving larger areas comprises deeper engraving on molds. Regarding these results, laser power of 2.5 W and 7.5 W showed up as being the most likely to produce semi-sphere like structures.

Furthermore, microstructures resultant from two similar designs were used to compare the theoretical diameter and pitch with the resultant ones, as well as to compare the resolution over vertical and horizontal directions. The first design is based on circles with a theoretical diameter of $200\ \mu\text{m}$ and a pitch of $150\ \mu\text{m}$, while the second design is based on circles with a theoretical diameter of $200\ \mu\text{m}$ and a pitch of $200\ \mu\text{m}$. To do so, molds were made using a laser power of $2.5\ \text{W}$ and $7.5\ \text{W}$, maintaining speed at $0.254\ \text{m/s}$ for both. Table 3.4 shows the general view of the resultant PDMS structures exhibiting nice homogeneity for each pattern, while highlighting the differences between pitches and diameters over horizontal and vertical directions. From the images one notices that each feature can easily be discerned even for the lower pitch, meaning that theoretical pitch of about $150\ \mu\text{m}$ is achievable with this technique.

Table 3.4: SEM images acquired of microstructured PDMS films. Images (a)-(h) result from molds engraved with a laser power of $2.5\ \text{W}$ and $0.254\ \text{m/s}$ laser speed for different pitches and diameters. Images (i)-(p) result from molds engraved with a laser power of $7.5\ \text{W}$ and $0.254\ \text{m/s}$ laser speed for different pitches and diameters.



As previously seen, measurements over both horizontal and vertical directions should be performed in order to thoroughly analyse features. Hence, all semi-spheres were measured over both directions of the engraving process. Table A.1 summarizes the measured

diameter and pitch of the fabricated features, showing that although diameter and pitch values were usually far from what was designed, the sum of diameter and pitch tends to be very close to the expected sum of the designed ones. This can be explained by the fact that laser beam melts more PDMS than it was designed, performing engravings much larger than expected, which is corroborated by the discrepancy, sometimes larger than 100 μm , on measured diameters. Therefore, pitch for its turn, shows to be much smaller

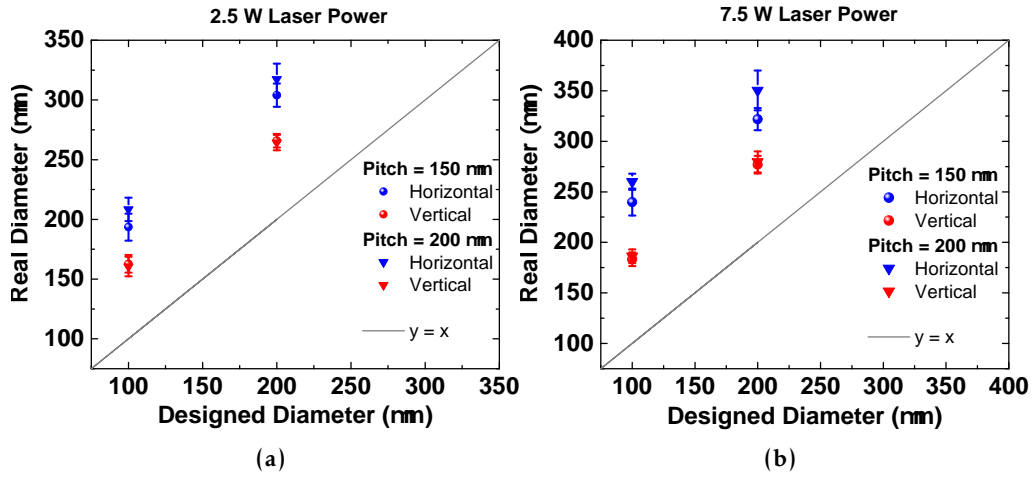


Figure 3.3: Real diameter of PDMS semi-spheres, measured over horizontal and vertical directions of laser engraving versus designed diameter in Adobe Illustrator, produced with a laser power of (a) 2.5 W or (b) 7.5 W. The lines $y = x$ illustrate a real diameter equal to the one designed. Values presented correspond to average values \pm standard deviation of a minimum of 15 measurements.

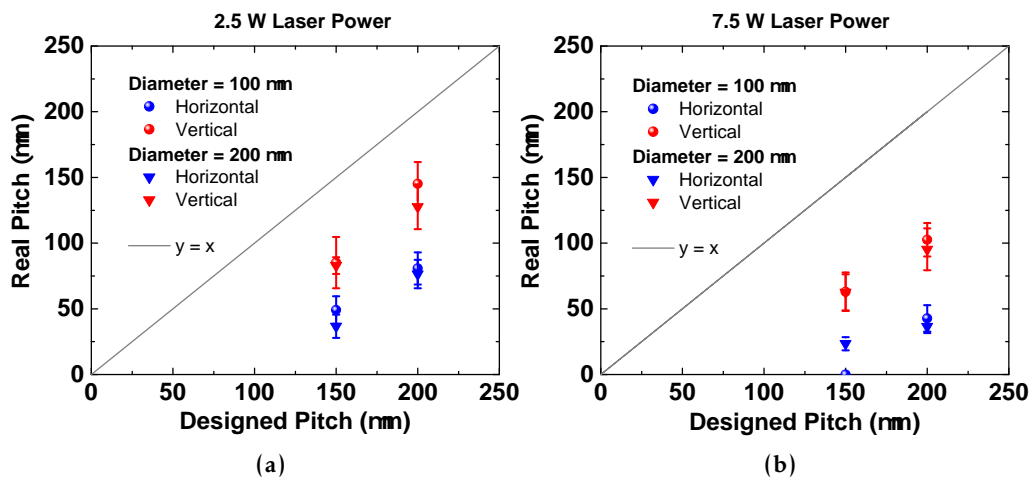


Figure 3.4: Real pitch between PDMS semi-spheres, measured over horizontal and vertical directions of laser engraving versus designed pitch in Adobe Illustrator, produced with a laser power of (a) 2.5 W or (b) 7.5 W. The lines $y = x$ illustrate a real pitch equal to the one designed. Values presented correspond to average values \pm standard deviation of a minimum of 15 measurements.

than expected to maintain the design. Laser engraving resolution in vertical direction is notably better than in horizontal direction once features measured in vertical direction of the laser engraving show values of diameter and pitch closer to the designed ones, as it is shown on Figure 3.3 and Figure 3.4, respectively.

As a result of all the explained before, the molds chosen for fabrication of PDMS membranes come as a combination of using designs with circles to be engraved on h-PDMS with a laser engraving machine on vector mode. The parameters chosen were 7.5 W of laser power and speed of 0.254 m/s, as with this combination more reproducible semi-sphere structures are achievable. Two molds using this combination of parameters were produced, both with theoretical diameters of 200 μm – the first with a pitch of 150 μm and the second with a pitch of 200 μm . Figure 3.5 shows the two molds produced and Figure 3.6 shows a microscope image of each PDMS mold that was used to fabricate membranes present in the studies further explained in this work, which were measured to have a thickness of 215 $\mu\text{m} \pm 19 \mu\text{m}$ (average values \pm standard deviation) corresponding to a minimum of 15 measurements.

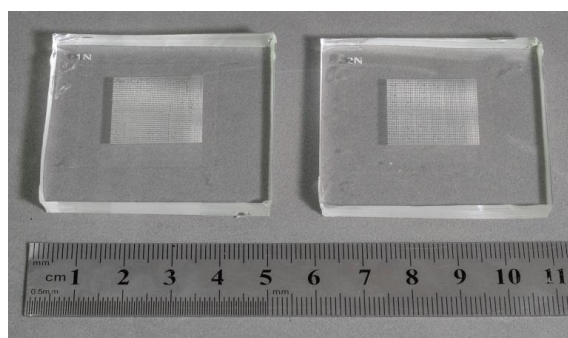


Figure 3.5: Molds produced for fabrication of membranes. Mold on the left designed with circles with 200 μm of diameter and pitch = 150 μm . Mold on the right designed with circles with 200 μm of diameter and pitch = 200 μm

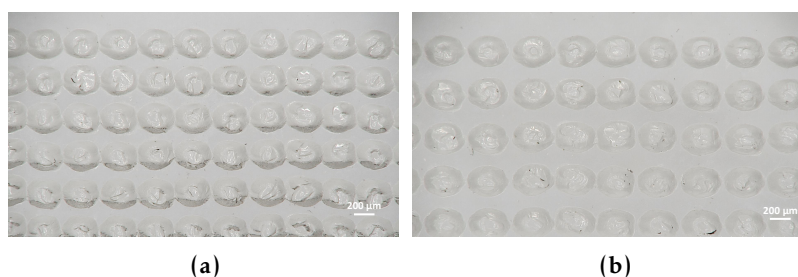


Figure 3.6: Microscope acquired images of the fabricated molds. (a) Mold designed with diameter = 200 μm and pitch = 150 μm . (b) Mold designed with diameter = 200 μm and pitch = 200 μm .

3.2 Ink Study

3.2.1 Carbon-ink dilution study

Studies over carbon-ink dilutions and number of layers were performed to further explore the best conductive film to fabricate piezoresistive sensors. Herein, **PMMA** was investigated as a coating layer between carbon-ink and **PDMS** to check if it could both improve the adhesion of carbon ink to **PDMS** and the final stability of the device. Firstly, to investigate the possibility of using less carbon-ink without compromising the good functionality of the piezoresistive sensors, sheet resistance of smooth carbon-coated **PDMS** and smooth carbon-coated **PDMS** with **PMMA** was measured by varying the dilution of the coating in water (100 wt %, 67 wt %, 50 wt %, 40 wt %). Figure 3.7 shows a comparison of sheet resistance between carbon-ink deposited on **PDMS** with and without **PMMA**. Both curves tend to decrease in sheet resistance as carbon-ink concentration in water increases, as expected. From this study it was found that sheet resistance for 50 wt % and 40 wt % dilutions, for both **PDMS** with and without **PMMA**, is excessively high for a conductive film, with average resistance values above 30 k Ω / \square . For films with approximately 67 wt

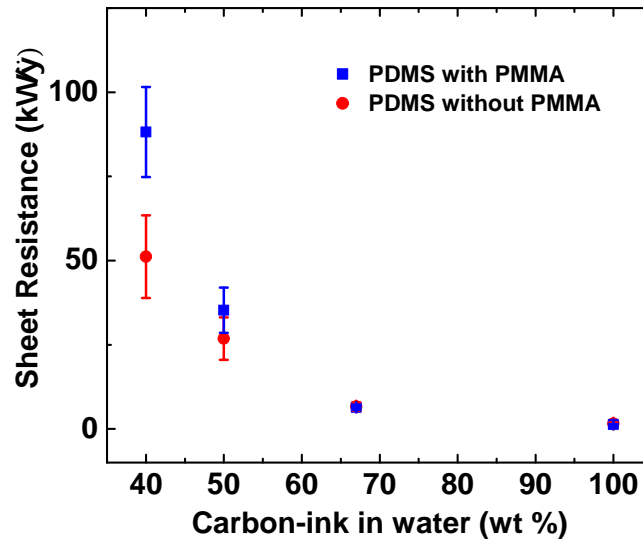


Figure 3.7: Sheet resistance of smooth carbon-coated **PMDS** and **PMMA**-coated **PDMS** for four different carbon-ink dilutions in water. Measurements presented here correspond to average values \pm average absolute deviation of a minimum of 3 measurements.

% dilution, the sheet resistance is (6.7 ± 1.2) k Ω / \square and (6.4 ± 0.8) k Ω / \square , respectively for smooth carbon-coated **PDMS** and smooth carbon-coated **PDMS** with **PMMA**.

Using a concentration of 100 wt % of carbon-ink ensures a sheet resistance of about (1.3 ± 0.1) k Ω / \square and (1.6 ± 0.3) k Ω / \square , respectively for **PDMS** with and without **PMMA**, which is suitable for the fabrication of piezoresistive pressure sensors. Figure 3.7 illustrates that 67 wt% and 100 wt% dilutions allow an easy replication of the membranes produced as the sheet resistance average values are deviated by a small error.

3.2.2 Ink layers study

To further understanding the relation between carbon coating layers and their behaviour on the device, a study comparing sheet resistance of different deposited layers using the dilutions of 67 wt% and 100 wt% was accomplished. Figure 3.8a shows a comparison of sheet resistance as a function of the number of layers for PDMS and PMMA-coated PDMS.

Regarding the 67 wt% dilution of carbon-ink on PDMS with PMMA, sheet resistance of one layer is approximately (6.4 ± 0.8) k Ω/\square . Sheet resistance, as expected, decreases with the number of carbon layers deposited by spin-coating as the amount of conductive coating increases. The deviation error also decreases which means that the conduction mechanism is becoming homogenous for the whole membrane. Both dilutions tend to a limit of sheet resistance with the increasing layers. Nevertheless, as expected, the 67 wt% dilution requires more stacked layers to reach the same values of sheet resistance of 100 wt%. Therefore, for 100 wt% dilution, there was no need to perform studies over more layers, once the values were already low enough. The sheet resistance on PDMS values are close to the ones with the same dilution on PMMA for both dilutions studied here, however, it appears to have higher deviation error, which means PMMA on PDMS seems to contribute for a greater stability of carbon coating adhesion.

The first carbon coating layer for all four curves shows a larger deviation error of sheet resistance than for all other layer depositions due to the heterogeneity of deposited carbon. This observation is corroborated by the deviation errors for thickness, which were also measured in this study.

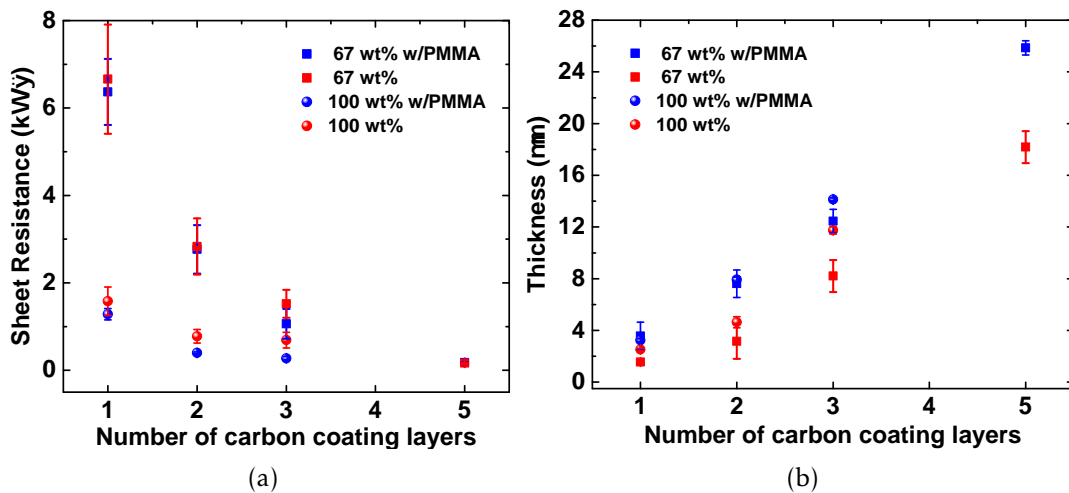


Figure 3.8: (a) Sheet resistance of 67 wt% and 100 wt% carbon coating dilutions in water on smooth PDMS films and PMMA-coated PDMS films with 1 to 5 layers of coating. (b) Thickness of 67 wt% and 100 wt% carbon coating on smooth PDMS films and PMMA-coated PDMS films with 1 to 5 layers of coating. Measurements presented here correspond to average values \pm average absolute deviation of a minimum of 3 measurements.

Thicknesses presented on Figure 3.8b were measured between the top of the coating

layers and the top of PDMS membranes, meaning that the presented thickness corresponds to the sum of every layer on PDMS, including PMMA, if applicable. This figure highlights a more linear behaviour for thickness in function of layer depositions on PMMA for both dilutions than for deposited layers on PDMS, which confirms that PMMA plays an important role on carbon coating adhesion.

Given that the purpose of this work is to produce thin and flexible membranes, a trade-off between thickness and resistance has to be reached. Although membranes coated with 100 wt% carbon coating show higher thickness, they also show relatively lower resistance when compared with membranes coated with 67 wt% carbon coating. Therefore, 100 wt% carbon coating dilution with only one coating layer was chosen over other dilutions once it presents a very reasonable value of sheet resistance and comprises the lowest thickness possible with this sheet resistance value.

3.2.3 Electrical Characterization of carbon-coated membranes

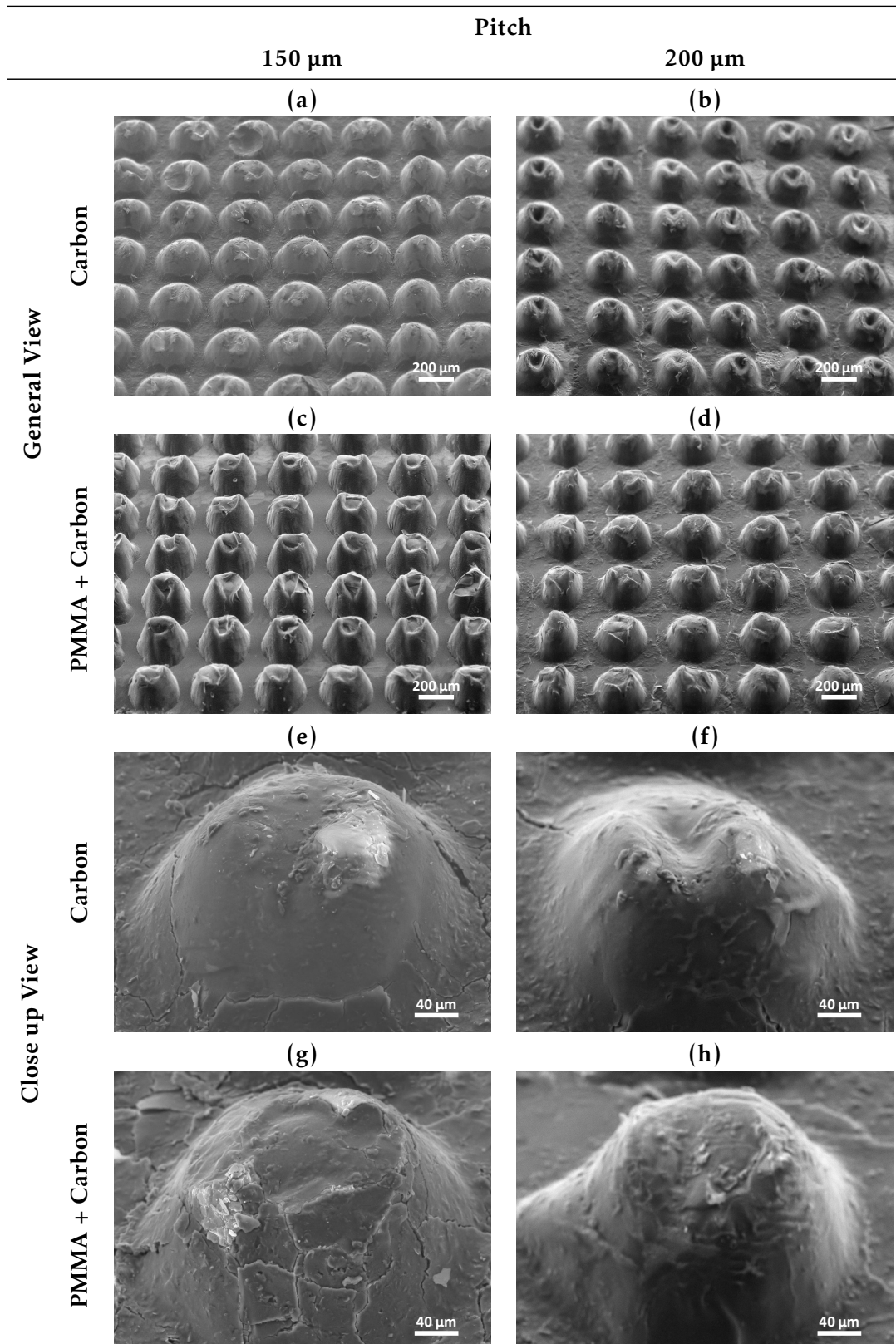
Moreover, microstructured membranes using the chosen carbon coating dilution were also electrically characterized to investigate the role of microstructures on membrane resistance. Figure B.1a shows results for four different membranes containing semi-spheres with a diameter of 200 μm and a pitch of 150 μm , whereas Figure B.1b results from the study for four different membranes with semi-spheres with a diameter of 200 μm and a pitch of 200 μm . Both figures prove the ohmic behaviour of carbon coating on membranes and therefore the same ohmic behaviour was expected for the whole device when current flows from a membrane to the other. Both figures allow the estimation of the average nominal resistance for each membrane pattern which is calculated to be $(1.2 \pm 0.4) \text{ k}\Omega/\square$ and $(1.2 \pm 0.2) \text{ k}\Omega/\square$ for microstructures with the lower pitch and the higher pitch, respectively.

3.2.4 Morphological Characterization of carbon-coated membranes

Microstructured carbon-coated membranes were also morphologically characterized using SEM, in order to analyse membrane's thickness, semi-spheres' diameter, pitch, and height as well as the homogeneity of carbon coating. Figure 3.5a to Figure 3.5d show a general view of the produced 200 μm diameter semi-spheres. All images show the engraving direction over the vertical direction as it becomes easier to contrast the pitch. Figure 3.5c and Figure 3.5d present semi-spheres with greater height due to the presence of PMMA on their structure, which can also be corroborated by measurements acquired of the dimensions of the microstructures present in Section C.

Overall, all images acquired show homogeneity over all structures, with semi-spheres perfectly aligned over both vertical and horizontal directions. When facing two membranes to produce a piezoresistive device, the pitch and diameters chosen for these patterns will promote the contact between both groups of semi-spheres, hence granting reproducibility over devices and possibly contributing for a lower nominal resistance due

Table 3.5: SEM images of microstructures produced on PDMS with carbon and PMMA + carbon coatings. Images (a)-(d) general view of aligned semi-spheres with a designed base diameter of 200 μm , with pitches of 150 μm - (a),(c) or 200 μm - (b),(d). Images (e)-(h) close up view of aligned semi-spheres with a designed base diameter of 200 μm , with pitches of 150 μm - (e),(g) or 200 μm - (f),(h).



to more contact spots for electrical current flowing. Figure 3.5e to Figure 3.5h show that both layers, PMMA and carbon coating, seem to spread homogeneously over PDMS surface and semi-spheres, once semi-sphere structures are not sharp enough to avoid coating to adhere there as well as it adheres in other substrate spots.

3.3 Homemade Pressure Applying System

Testing the fabricated devices comprises measuring the device's piezoresistive signal in response to an applied pressure and comparing fabricated devices requires the application of the same pressure on every single sample. Therefore, and to overcome the lack of systems applying a reproducible force, a homemade system with this purpose was built. In Figure 3.9, a simplified block diagram illustrates the system principal components and functions, consisting in an Arduino to control the entire system, a stepper motor driver, a liquid crystal display (LCD) display to act as user interface (allowing to define frequency and pressure for measurements as well as to set the tip on the desired spot), and the stepper motor Motor Nema17.

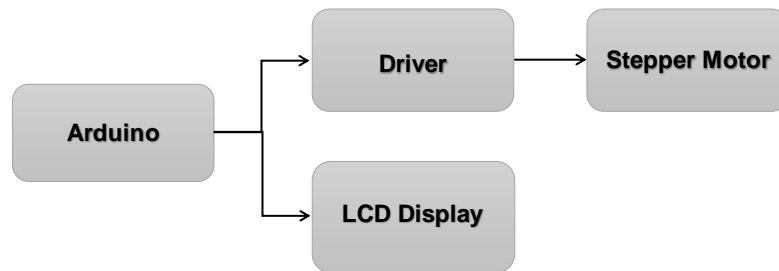


Figure 3.9: Block diagram representing the blocks constituting the system built - an arduino controlling the stepper motor driver and the LDC display.

Figure 3.10 shows the built circuit used for the developed system. Figure 3.11 represents the developed system, from where one can clearly realize each component and from where one may see that the critical element of the apparatus is the conversion of radial force in vertical force and what enables this is the motor which, once in movement, makes the arm connected to it to move vertically, applying a force that is directly proportional to the displacement of the tip of the arm. This system, among other components, is provided with a piezoelectric sensor (piezoelectric coefficient, $d_{33} = 800$ pC/N and a capacity, $C = 20$ nF) capable of detecting a response signal which can be then converted to force (N), allowing a continuous monitoring of the applied pressure on the fabricated devices. The tip of the system, element which is in contact with devices, consists in a rubber, mechanically characterized with a Young's Modulus of 15 MPa.

The black-painted components present in Figure 3.11 were designed in the 3D modeling computer program SketchUp, as seen in Section D and subsequently printed in a 3D printer Prusa i3. The acrylic components were cut in the laser engraving machine in designs previously drawn in Adobe Illustrator (2015.0.0). The section of the code

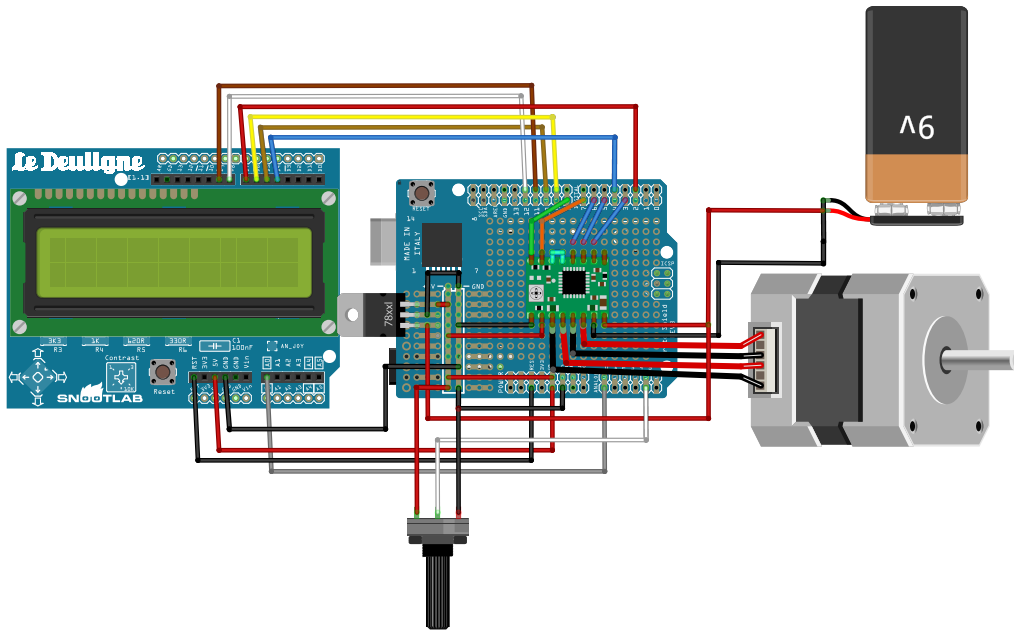


Figure 3.10: Circuit design for the development of the system. The circuit consists in an Arduino board controlling a stepper motor driver and a LCD. A 9 V voltage is the source of the system, used to power the motor and to power Arduino after being converted to 5 V by a 7805 voltage regulator. A potentiometer is also connected to the arduino to help in user interface.

responsible for the movement of the stepper motor and therefore, the movement of the tip, is also presented in Section D as well as a schematic of the whole developed system with indication of each component. Moreover, in order to have a clear signal from the piezoelectric sensor, a RC Low-Pass Filter with Op Amp Buffer with 3 poles represented in Section D, was connected to the system.

In the conformation exhibited in Figure 3.11, this homemade system is able to provide pressures applied in frequencies from 0.5 Hz to 20 Hz with electrical signals from both piezoelectric sensor and piezoresistive fabricated devices simultaneously monitored and recorded on an oscilloscope. The range of pressure being applied by the machine can be adjusted depending on what is the final object applying the force, meaning that, using materials with larger area than the rubber, one can reach lower pressures. Figure 3.12 shows the output signal of the piezoelectric device, responding to stimulus performed by the machine in order to ascertain the limits of the system mounted as previously shown. Figure 3.12a represents the sinusoidal pressure being applied on the piezoelectric sensor by a vertical displacement of the rubber on the sensor of 70 μm , with the maximum frequency possible for the apparatus. This displacement results in a maximum applied pressure of approximately 130 kPa. Figure 3.12b represents the same displacement but with lower frequency and applying a maximum pressure of approximately 600 kPa. The change of wave type to an approximately square wave can be explained by the fact that the motor to perform a displacement of 70 μm , only rotates 1 step and at low frequencies

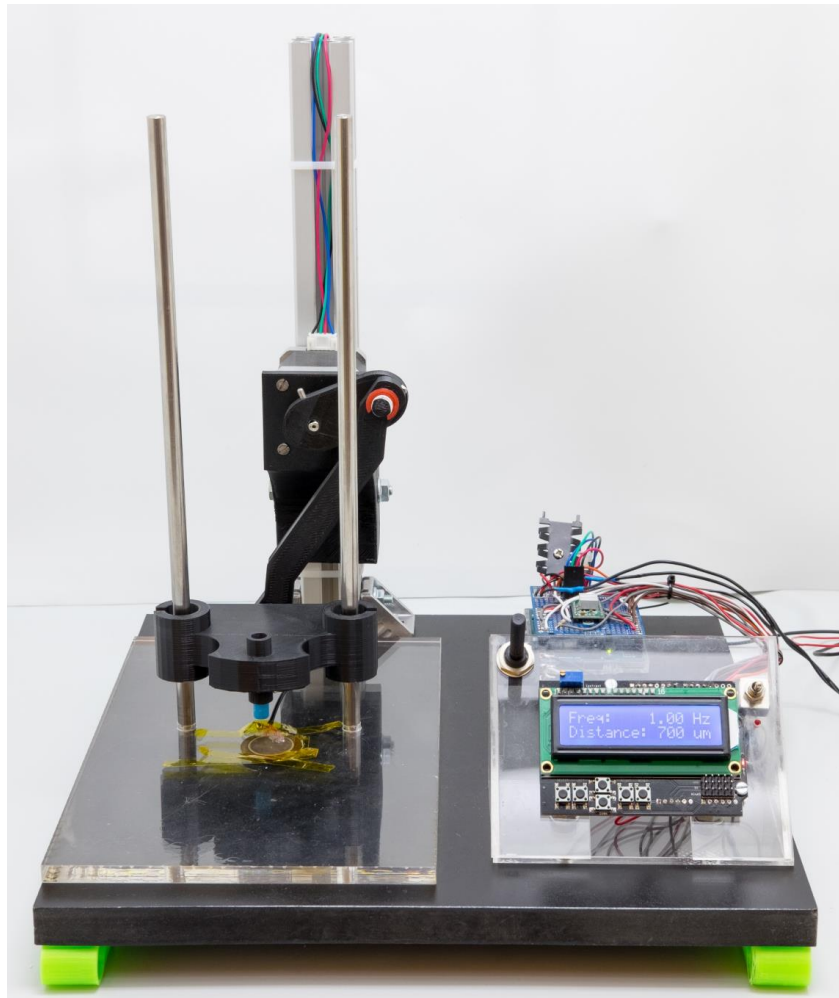


Figure 3.11: Picture representing the pressure applying system developed.

1 step seems to be insufficient for this time interval and therefore motor stays immobile for most of the time. Figure 3.12c represents a vertical displacement of $700\ \mu\text{m}$ with a frequency of $20\ \text{Hz}$, corresponding to an applied pressure of approximately $1.4\ \text{MPa}$, which consists in an increase in pressure of about 10 times when compared to a displacement 10 times lower with the same frequency. Although the values seem very conformal with the expected, the stepper motor finds difficult succeeding in performing the desired frequency as this seems to be a very high displacement for the frequency of $20\ \text{Hz}$, as seen in the plot. Figure 3.12d also results from a vertical displacement of $700\ \mu\text{m}$ but with a frequency of $0.5\ \text{Hz}$. The maximum pressure applied for this displacement is $5.1\ \text{MPa}$, consisting in a increase of pressure of about 9 times when compared with a displacement 10 times lower with the same frequency. From these results, it was proven the good behaviour of the system on the frequencies tested. The results also showed that the minimum pressure applied for this conformation was approximately $130\ \text{kPa}$ and the maximum was approximately $5.1\ \text{MPa}$.

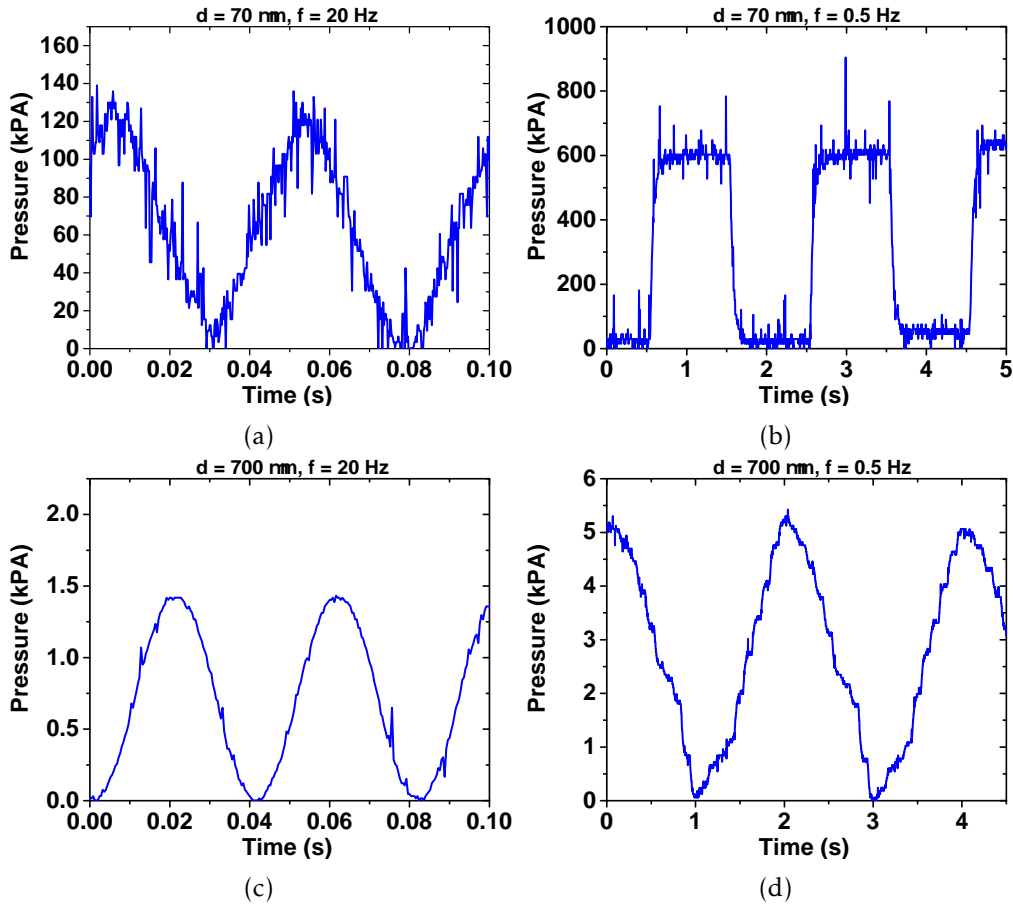


Figure 3.12: Pressure applied on piezoelectric sensor versus time. (a) Displacement of $70 \mu\text{m}$ and frequency of 20 Hz. (b) Displacement of $70 \mu\text{m}$ and frequency of 0.5 Hz. (c) Displacement of $700 \mu\text{m}$ and frequency of 20 Hz. (d) Displacement of $700 \mu\text{m}$ and frequency of 0.5 Hz.

3.4 Electrical Characterization of Devices

The fabricated devices were submitted to tests over sensitivity, nominal resistance and ohmic-like contact. First of all, sealing two membranes with the microstructure domain facing each other is a dominant factor in device fabrication, because the contact between two opposite semi-spheres caused by an external loading is what generates a change in the electrical resistance signal. Consequently, for a good reproducibility of devices, membranes require to be similarly sealed. Tests on sealing membranes with and without a window of Kapton tape acting as a spacer between the membranes were also performed, showing no evidence of improvements in using the tape as devices' sensibility is not influenced by it. Tests on I-V curves of the fabricated devices were conducted, exhibiting sheet resistance of approximately $1 \text{ k}\Omega/\square$ proving the good tendency of devices to ohmically conduct current from one membrane to the other, as shown on Figure 3.13.

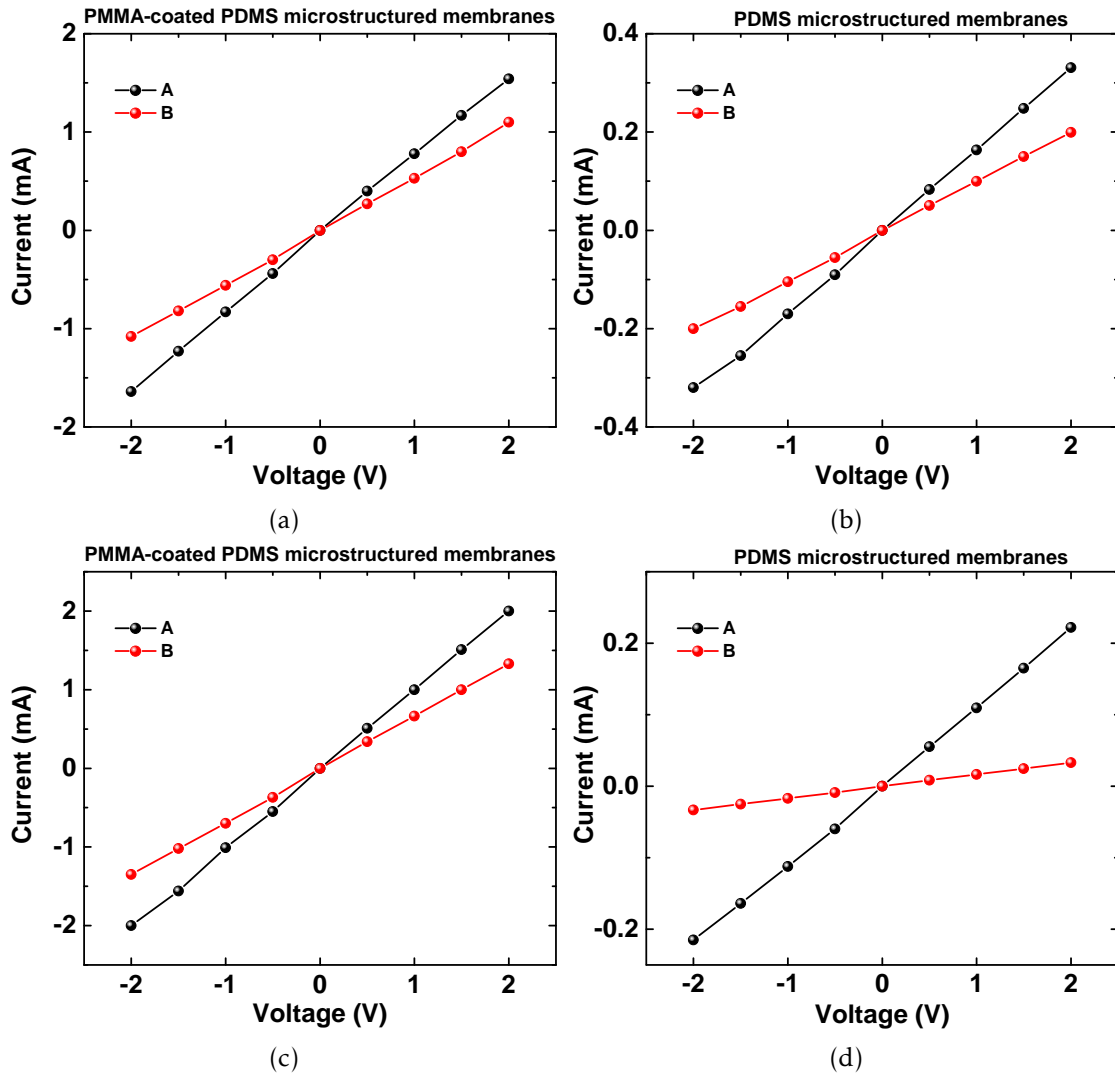


Figure 3.13: Voltage sweep from -2 to 2 V proving the ohmic behaviour of two devices produced with (a) PMMA-coated PDMS membrane with semi-spheres with a pitch of 150 μm . (b) PDMS membrane with semi-spheres with a pitch of 150 μm . (c) PMMA-coated PDMS membrane with semi-spheres with a pitch of 200 μm . (d) PDMS membrane with semi-spheres with a pitch of 200 μm .

Furthermore, to better understand the signal over time in response to applied pressure, output signal was acquired as function of a pressure range, at the frequency of 1 Hz. Figure 3.14 shows the output signal for each type of fabricated sensor. Herein, one observes the good output signal reproducibility over cycles, confirming the good stability of the device, and proving that the design of the device is suitable for this type of applications. As seen in Figure 3.14c, sensors fabricated with PMMA coating on PDMS with a pitch of 200 μm present a higher output signal for the same pressure than other fabricated sensors. Both curves on each graph present a phase difference of about 0.01° to 0.8° which may be introduced by the assembled system composed by the electronic components and the motor, even so, this does not seem to cause interference to the device's

performance.

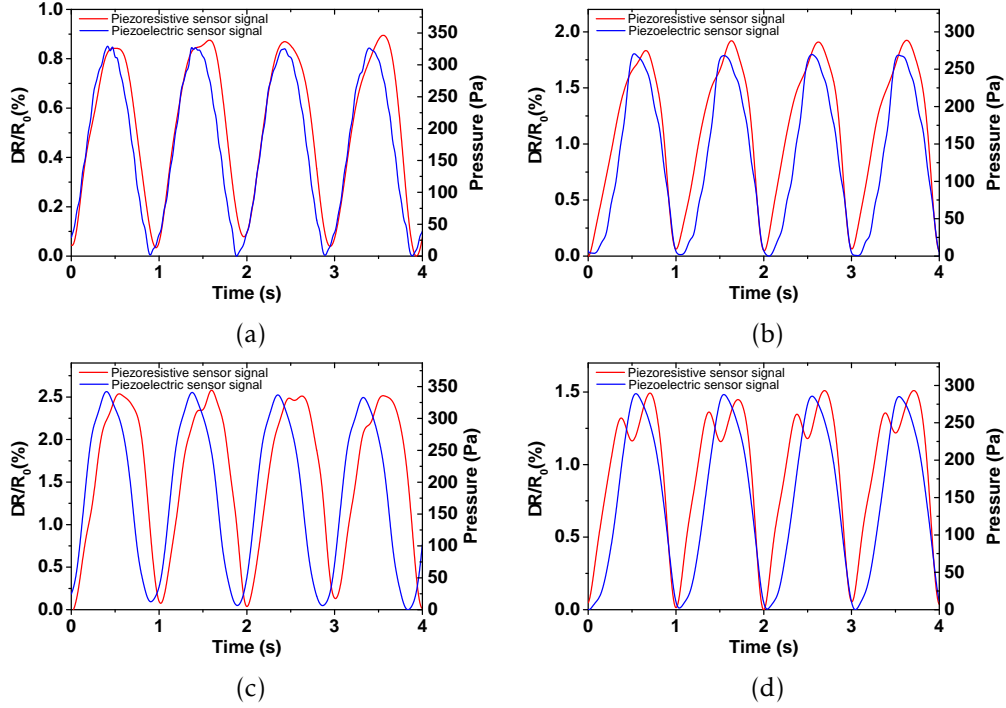


Figure 3.14: Resistance changes in response to applied pressure over time (a) PMMA-coated PDMS membrane with semi-spheres with a pitch of 150 μm . (b) PDMS membrane with semi-spheres with a pitch of 150 μm . (c) PMMA-coated PDMS membrane with semi-spheres with a pitch of 200 μm . (d) PDMS membrane with semi-spheres with a pitch of 200 μm .

Moreover, Figure 3.15 shows the approximately linear relation between $\Delta R/R_0$ and the applied pressure (regarding the principle illustrated in Figure E.1, Section E), for the two designs on membranes with and without PMMA, from where one may calculate a sensitivity.

Sensitivities of $S = 4.9 \times 10^{-2} \text{ kPa}^{-1}$ for external pressures ranging from 9 Pa to 330 Pa for PMMA-coated PDMS containing semi-spheres with a pitch of 150 μm , $S = 1.3 \times 10^{-1} \text{ kPa}^{-1}$ for external pressures ranging from 5 Pa to 360 Pa for PDMS containing semi-spheres with a pitch of 150 μm , $S = 2.4 \times 10^{-1} \text{ kPa}^{-1}$ for external pressures ranging from 4 Pa to 150 Pa for PMMA-coated PDMS containing semi-spheres with a pitch of 200 μm , and $S = 9.2 \times 10^{-2} \text{ kPa}^{-1}$ for external pressures ranging from 10 Pa to 340 Pa for PDMS containing semi-spheres with a pitch of 200 μm , were acquired. In Section F a signal response to the approximately same applied pressure, at both a frequency of 1 Hz and 15 Hz are shown, proving that the fabricated sensors maintain their performance for this range of frequencies as the relative resistance change stays identical.

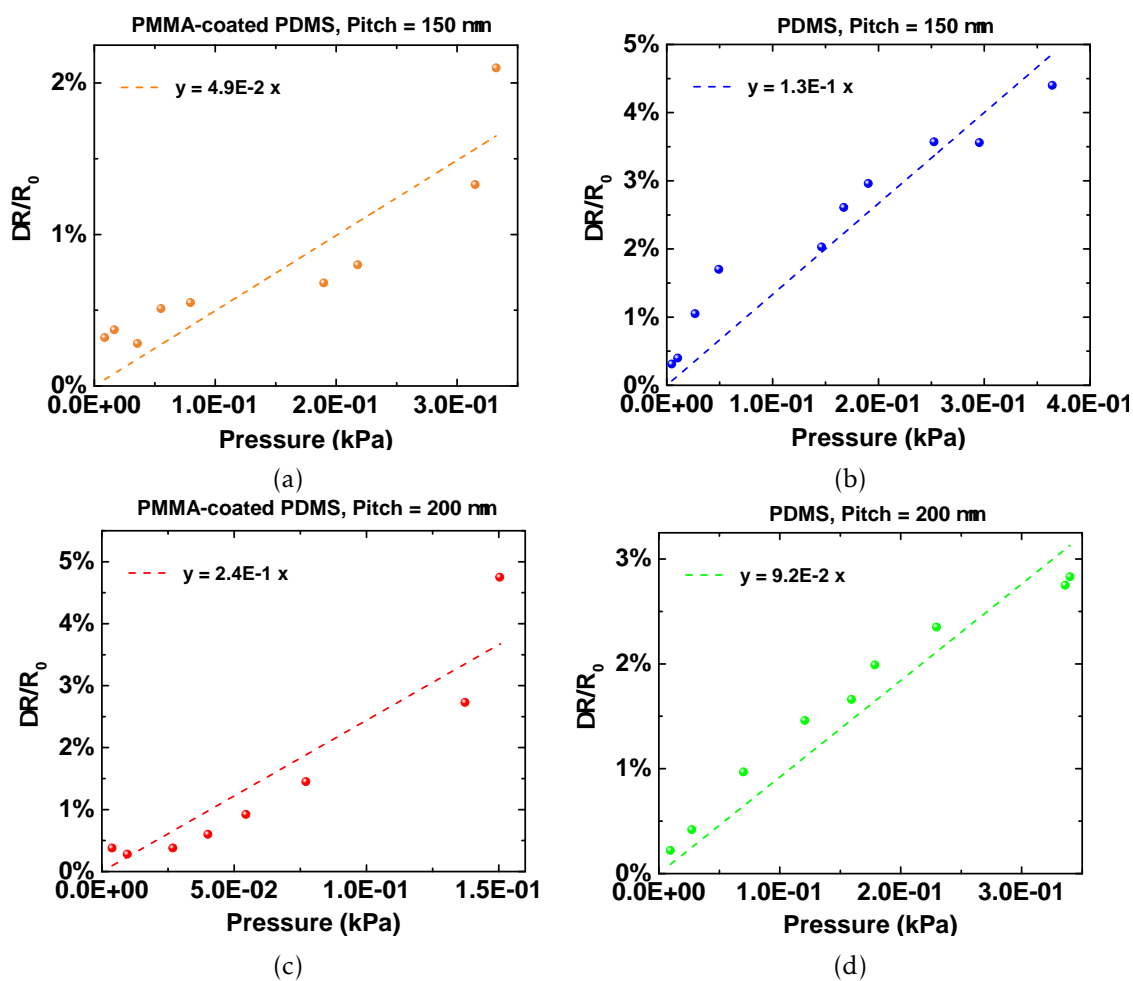


Figure 3.15: Resistance response to different pressures. Dot line is a linear regression from which the sensitivity of each device is extracted. (a) PMMA-coated PDMS membrane with semi-spheres with a pitch of 150 μm . (b) PDMS membrane with semi-spheres with a pitch of 150 μm . (c) PMMA-coated PDMS membrane with semi-spheres with a pitch of 200 μm . (d) PDMS membrane with semi-spheres with a pitch of 200 μm .

Conclusions and future perspectives

In the present work, the major objective was to develop a simple and low-cost method for fabrication of carbon-coated PDMS with uniformly microstructured patterns. To accomplish so, a thin PDMS film was microstructured with semi-spheres, and posteriorly covered by a flexible carbon coating.

As previously seen, the combination of laser engraving parameters, the design of microstructures, and the type of mold showed to be of significant importance in order to obtain the desired microstructures on the fabricated PDMS membranes. One major conclusion of this work is that the ideal combination to obtain semi-spheres is to use designs with circles engraved on h-PDMS molds with laser engraving machine on vector mode. Although the real values of pitch and diameter do not maintain fidelity to the designed values, this method allows a fabrication of controlled and reproducible semi-sphere-like structures. Semi-sphere dimensions such as pitch size, height and diameter have a serious effect on the performance of the pressure sensors as the microstructures play the most important role on the variation of contact area upon pressure, affecting the pressure sensors sensitivity. Other conclusion of this work is that the laser engraving machine has better resolution over vertical direction of laser engraving than over horizontal direction, as real values of semi-sphere' pitch and diameter tend to be much closer to the values designed in software, when measured on the vertical direction. Regarding studies with the active layer material, carbon coating, the results showed that using one single coating layer of 100 wt % carbon coating dilution would be preferred over using various layers of lower dilutions, as it requires less work and time consumption and ensures lower sheet resistances and thickness.

A homemade pressure applying system was developed in order to electrically characterize the fabricated devices. This system can provide pressures in frequencies from 0.5 Hz to 20 Hz, and the range of the applied pressure can be easily adjusted depending on what is the final object applying the force. For example, an object with larger area will apply lower pressure. Further improvements on this system could be made by changing the 3D printed components to carbon fiber ones and changing the rubber tip to a softer material with larger area.

In what concerns the pressure sensors, devices comprising a PMMA layer between PDMS and carbon coating were fabricated in order to investigate PMMA adhesion properties. In terms of sensitivity, the sensor with higher sensitivity was the one fabricated with a larger pitch and with a PMMA layer but at the same time, the lower sensitivity was found in the sensor with a PMMA layer but with lower pitch. Such observation can be derived from the fact that for the lower pitch, the presence of an extra layer (PMMA) and, therefore, additional thickness, would mean a spoilage of the sensing properties as

the interlocked domain may act as a smooth film, instead of increasing the contact area between both microstructured films.

The higher sensitivity reached was $2.4 \times 10^{-1} \text{ kPa}^{-1}$ for external pressures ranging from 4 Pa to 150 Pa. In fact, one expects that the use of thinner PDMS films enhances the sensitivity of the full device. These sensors were estimated with a price of 0.351 € of materials costs, as seen in Section G.

In conclusion, the approaches presented here contribute to a new direction of flexible, low-cost, and easily assembled for future health monitoring devices because despite the fast progress in e-skin devices, there is room for investigation in the field of low-cost and low power consumption sensors, where the integration of multiple other sensing properties, namely temperature, shear, and vibration, is also appealing. Other appealing functionalities such as biocompatibility, self-healing also need further attention for the implementation in e-skin to fully mimic its organic parallel. Self-powering, for example, also constitutes a demand once it would allow an autonomy degree which is not possible with an immovable power supply. This could be achieved by adding, for example, solar cells, batteries and wireless antennas.

Based on the key features in the present work, namely the microstructures, upcoming works will require attention on improving the sensitivity by using newly developed functional materials and optimization of device geometries.

Bibliography

- [1] M. L. Hammock, A. Chortos, B. C.-K. Tee, J. B.-H. Tok, and Z. Bao. “25th anniversary article: the evolution of electronic skin (e-skin): a brief history, design considerations, and recent progress”. In: *Advanced Materials* 25.42 (2013), pp. 5997–6038.
- [2] P. Delmas, J. Hao, and L. Rodat-Despoix. “Molecular mechanisms of mechanotransduction in mammalian sensory neurons”. In: *Nature reviews. Neuroscience* 12.3 (2011), pp. 139–153.
- [3] J. Kim, M. Lee, H. J. Shim, R. Ghaffari, H. R. Cho, D. Son, Y. H. Jung, M. Soh, C. Choi, S. Jung, et al. “Stretchable silicon nanoribbon electronics for skin prosthesis”. In: *Nature communications* 5 (2014), pp. 1–11.
- [4] S. Bauer, S. Bauer-Gogonea, I. Graz, M. Kaltenbrunner, C. Keplinger, and R. Schwödiauer. “25th anniversary article: a soft future: from robots and sensor skin to energy harvesters”. In: *Advanced Materials* 26.1 (2014), pp. 149–162.
- [5] D. Son, J. Lee, S. Qiao, R. Ghaffari, J. Kim, J. E. Lee, C. Song, S. J. Kim, D. J. Lee, S. W. Jun, et al. “Multifunctional wearable devices for diagnosis and therapy of movement disorders”. In: *Nature nanotechnology* 9.5 (2014), pp. 397–404.
- [6] G. Schwartz, B. C. Tee, J. Mei, A. L. Appleton, D. H. Kim, H. Wang, and Z. Bao. “Flexible polymer transistors with high pressure sensitivity for application in electronic skin and health monitoring”. In: *Nature communications* 4 (2013), pp. 1–8.
- [7] C. Pang, G.-Y. Lee, T.-i. Kim, S. M. Kim, H. N. Kim, S.-H. Ahn, and K.-Y. Suh. “A flexible and highly sensitive strain-gauge sensor using reversible interlocking of nanofibres”. In: *Nature materials* 11.9 (2012), pp. 1–7.
- [8] J. Park, Y. Lee, J. Hong, M. Ha, Y.-D. Jung, H. Lim, S. Y. Kim, and H. Ko. “Giant tunneling piezoresistance of composite elastomers with interlocked microdome arrays for ultrasensitive and multimodal electronic skins”. In: *ACS nano* 8.5 (2014), pp. 4689–4697.
- [9] S. Gong, W. Schwalb, Y. Wang, Y. Chen, Y. Tang, J. Si, B. Shirinzadeh, and W. Cheng. “A wearable and highly sensitive pressure sensor with ultrathin gold nanowires”. In: *Nature communications* 5 (2014), pp. 1–8.
- [10] D. J. Lipomi, M. Vosgueritchian, B. C. Tee, S. L. Hellstrom, J. A. Lee, C. H. Fox, and Z. Bao. “Skin-like pressure and strain sensors based on transparent elastic films of carbon nanotubes”. In: *Nature nanotechnology* 6.12 (2011), pp. 788–792.
- [11] Y. Zang, F. Zhang, D. Huang, X. Gao, C.-a. Di, and D. Zhu. “Flexible suspended gate organic thin-film transistors for ultra-sensitive pressure detection”. In: *Nature communications* 6 (2015), pp. 1–9.

- [12] S. C. Mannsfeld, B. C. Tee, R. M. Stoltenberg, C. V. H. Chen, S. Barman, B. V. Muir, A. N. Sokolov, C. Reese, and Z. Bao. “Highly sensitive flexible pressure sensors with microstructured rubber dielectric layers”. In: *Nature materials* 9.10 (2010), pp. 859–864.
- [13] C. Dagdeviren, Y. Su, P. Joe, R. Yona, Y. Liu, Y.-S. Kim, Y. Huang, A. R. Damadoran, J. Xia, L. W. Martin, et al. “Conformable amplified lead zirconate titanate sensors with enhanced piezoelectric response for cutaneous pressure monitoring”. In: *Nature communications* 5 (2014), pp. 1–9.
- [14] Z. Pi, J. Zhang, C. Wen, Z.-b. Zhang, and D. Wu. “Flexible piezoelectric nanogenerator made of poly (vinylidene fluoride-co-trifluoroethylene)(PVDF-TrFE) thin film”. In: *Nano Energy* 7 (2014), pp. 33–41.
- [15] L. Persano, C. Dagdeviren, Y. Su, Y. Zhang, S. Girardo, D. Pisignano, Y. Huang, and J. A. Rogers. “High performance piezoelectric devices based on aligned arrays of nanofibers of poly [(vinylidene fluoride-co-trifluoroethylene)]”. In: *arXiv preprint arXiv:1309.7166* (2013).
- [16] F.-R. Fan, L. Lin, G. Zhu, W. Wu, R. Zhang, and Z. L. Wang. “Transparent triboelectric nanogenerators and self-powered pressure sensors based on micropatterned plastic films”. In: *Nano letters* 12.6 (2012), pp. 3109–3114.
- [17] G. Zhu, W. Q. Yang, T. Zhang, Q. Jing, J. Chen, Y. S. Zhou, P. Bai, and Z. L. Wang. “Self-powered, ultrasensitive, flexible tactile sensors based on contact electrification”. In: *Nano letters* 14.6 (2014), pp. 3208–3213.
- [18] L. Lin, Y. Xie, S. Wang, W. Wu, S. Niu, X. Wen, and Z. L. Wang. “Triboelectric active sensor array for self-powered static and dynamic pressure detection and tactile imaging”. In: *ACS nano* 7.9 (2013), pp. 8266–8274.
- [19] Y. Zang, F. Zhang, C.-a. Di, and D. Zhu. “Advances of flexible pressure sensors toward artificial intelligence and health care applications”. In: *Materials Horizons* 2.2 (2015), pp. 140–156.
- [20] A. D. McNaught and A. D. McNaught. *Compendium of chemical terminology*. Vol. 1669. Blackwell Science Oxford, 1997.
- [21] S. Xu, Y. Qin, C. Xu, Y. Wei, R. Yang, and Z. L. Wang. “Self-powered nanowire devices”. In: *Nature nanotechnology* 5.5 (2010), pp. 366–373.
- [22] C. Pan, L. Dong, G. Zhu, S. Niu, R. Yu, Q. Yang, Y. Liu, and Z. L. Wang. “High-resolution electroluminescent imaging of pressure distribution using a piezoelectric nanowire LED array”. In: *Nature Photonics* 7.9 (2013), pp. 752–758.
- [23] R. D. P. Wong, J. D. Posner, and V. J. Santos. “Flexible microfluidic normal force sensor skin for tactile feedback”. In: *Sensors and Actuators A: Physical* 179 (2012), pp. 62–69.

-
- [24] J. A. Dobrzynska and M. A. Gijs. “Flexible polyimide-based force sensor”. In: *Sensors and Actuators A: Physical* 173.1 (2012), pp. 127–135.
- [25] R. Puers. “Capacitive sensors: when and how to use them”. In: *Sensors and Actuators A: Physical* 37 (1993), pp. 93–105.
- [26] M.-Y. Cheng, C.-L. Lin, Y.-T. Lai, and Y.-J. Yang. “A polymer-based capacitive sensing array for normal and shear force measurement”. In: *Sensors* 10.11 (2010), pp. 10211–10225.
- [27] L. Pan, A. Chortos, G. Yu, Y. Wang, S. Isaacson, R. Allen, Y. Shi, R. Dauskardt, and Z. Bao. “An ultra-sensitive resistive pressure sensor based on hollow-sphere microstructure induced elasticity in conducting polymer film”. In: *Nature communications* 5 (2014), pp. 1–8.
- [28] J. G. Dabling, A. Filatov, and J. W. Wheeler. “Static and cyclic performance evaluation of sensors for human interface pressure measurement”. In: *Engineering in Medicine and Biology Society (EMBC), 2012 Annual International Conference of the IEEE*. IEEE. 2012, pp. 162–165.
- [29] T. Yamada, Y. Hayamizu, Y. Yamamoto, Y. Yomogida, A. Izadi-Najafabadi, D. N. Futaba, and K. Hata. “A stretchable carbon nanotube strain sensor for human-motion detection”. In: *Nature nanotechnology* 6.5 (2011), pp. 296–301.
- [30] X. Wang, L. Dong, H. Zhang, R. Yu, C. Pan, and Z. L. Wang. “Recent progress in electronic skin”. In: *Advanced Science* 2.10 (2015).
- [31] Y. Kim, J. Zhu, B. Yeom, M. Di Prima, X. Su, J.-G. Kim, S. J. Yoo, C. Uher, and N. A. Kotov. “Stretchable nanoparticle conductors with self-organized conductive pathways”. In: *Nature* 500.7460 (2013), pp. 59–63.
- [32] D.-H. Kim, J. Xiao, J. Song, Y. Huang, and J. A. Rogers. “Stretchable, curvilinear electronics based on inorganic materials”. In: *Advanced Materials* 22.19 (2010), pp. 2108–2124.
- [33] F. Xu and Y. Zhu. “Highly conductive and stretchable silver nanowire conductors”. In: *Advanced materials* 24.37 (2012), pp. 5117–5122.
- [34] Y.-L. Park, B.-R. Chen, and R. J. Wood. “Design and fabrication of soft artificial skin using embedded microchannels and liquid conductors”. In: *IEEE Sensors Journal* 12.8 (2012), pp. 2711–2718.
- [35] X. Wang, Y. Gu, Z. Xiong, Z. Cui, and T. Zhang. “Silk-molded flexible, ultrasensitive, and highly stable electronic skin for monitoring human physiological signals”. In: *Advanced Materials* 26.9 (2014), pp. 1336–1342.
- [36] C.-L. Choong, M.-B. Shim, B.-S. Lee, S. Jeon, D.-S. Ko, T.-H. Kang, J. Bae, S. H. Lee, K.-E. Byun, J. Im, et al. “Highly stretchable resistive pressure sensors using a conductive elastomeric composite on a micropyramid array”. In: *Advanced materials* 26.21 (2014), pp. 3451–3458.

- [37] G. Y. Bae, S. W. Pak, D. Kim, G. Lee, D. H. Kim, Y. Chung, and K. Cho. "Linearly and Highly Pressure-Sensitive Electronic Skin Based on a Bioinspired Hierarchical Structural Array". In: *Advanced Materials* 28.26 (2016), pp. 5300–5306.
- [38] C. O. Chey, X. Liu, H. Alnoor, O. Nur, and M. Willander. "Fast piezoresistive sensor and UV photodetector based on Mn-doped ZnO nanorods". In: *physica status solidi (RRL)-Rapid Research Letters* 9.1 (2015), pp. 87–91.
- [39] S. Chun, Y. Kim, H.-S. Oh, G. Bae, and W. Park. "A highly sensitive pressure sensor using a double-layered graphene structure for tactile sensing". In: *Nanoscale* 7.27 (2015), pp. 11652–11659.
- [40] X. Yin, T. Vinod, and R. Jelinek. "A flexible high-sensitivity piezoresistive sensor comprising a Au nanoribbon-coated polymer sponge". In: *Journal of Materials Chemistry C* 3.35 (2015), pp. 9247–9252.
- [41] S. Wagner and S. Bauer. "Materials for stretchable electronics". In: *Mrs Bulletin* 37.3 (2012), pp. 207–213.
- [42] K. Kuribara, H. Wang, N. Uchiyama, K. Fukuda, T. Yokota, U. Zschieschang, C. Jaye, D. Fischer, H. Klauk, T. Yamamoto, et al. "Organic transistors with high thermal stability for medical applications". In: *Nature communications* 3 (2012), pp. 1–7.
- [43] M. Kaltenbrunner, T. Sekitani, J. Reeder, T. Yokota, K. Kuribara, T. Tokuhara, M. Drack, R. Schwödiauer, I. Graz, S. Bauer-Gogonea, et al. "An ultra-lightweight design for imperceptible plastic electronics". In: *Nature* 499.7459 (2013), pp. 458–465.
- [44] Y. Hwang, O. H. Paydar, and R. N. Candler. "3D printed molds for non-planar PDMS microfluidic channels". In: *Sensors and Actuators A: Physical* 226 (2015), pp. 137–142.
- [45] S. K. Sia and G. M. Whitesides. "Microfluidic devices fabricated in poly (dimethylsiloxane) for biological studies". In: *Electrophoresis* 24.21 (2003), pp. 3563–3576.
- [46] T. Sekitani, U. Zschieschang, H. Klauk, and T. Someya. "Flexible organic transistors and circuits with extreme bending stability". In: *Nature materials* 9.12 (2010), pp. 1015–1022.
- [47] M. Park, J. Im, M. Shin, Y. Min, J. Park, H. Cho, S. Park, M.-B. Shim, S. Jeon, D.-Y. Chung, et al. "Highly stretchable electric circuits from a composite material of silver nanoparticles and elastomeric fibres". In: *Nature nanotechnology* 7.12 (2012), pp. 803–809.
- [48] L. Hu, M. Pasta, F. La Mantia, L. Cui, S. Jeong, H. D. Deshazer, J. W. Choi, S. M. Han, and Y. Cui. "Stretchable, porous, and conductive energy textiles". In: *Nano letters* 10.2 (2010), pp. 708–714.

- [49] S. Merilampi, T Laine-Ma, and P. Ruuskanen. “The characterization of electrically conductive silver ink patterns on flexible substrates”. In: *Microelectronics reliability* 49.7 (2009), pp. 782–790.
- [50] Q. Sun, D. H. Kim, S. S. Park, N. Y. Lee, Y. Zhang, J. H. Lee, K. Cho, and J. H. Cho. “Transparent, Low-Power Pressure Sensor Matrix Based on Coplanar-Gate Graphene Transistors”. In: *Advanced Materials* 26.27 (2014), pp. 4735–4740.
- [51] S. Park, M. Vosguerichian, and Z. Bao. “A review of fabrication and applications of carbon nanotube film-based flexible electronics”. In: *Nanoscale* 5.5 (2013), pp. 1727–1752.
- [52] M. Moniruzzaman and K. I. Winey. “Polymer nanocomposites containing carbon nanotubes”. In: *Macromolecules* 39.16 (2006), pp. 5194–5205.
- [53] M.-L. Seol, J.-H. Woo, D.-I. Lee, H. Im, J. Hur, and Y.-K. Choi. “Nature-Replicated Nano-in-Micro Structures for Triboelectric Energy Harvesting”. In: *Small* 10.19 (2014), pp. 3887–3894.

Semi-sphere's dimensions measurements

Table A.1: Semi-spheres real diameter and real pitch measured on horizontal and vertical directions for each pitch and laser power tested. Values presented correspond to average values \pm standard deviation of a minimum of 15 measurements.

		Horizontal Direction				Vertical Direction			
Designed Pitch (μm)		150		200		150		200	
Designed Diameter (μm)		100	200	100	200	100	200	100	200
2.5 W	Real Diameter (μm)	194 \pm 11	304 \pm 10	208 \pm 10	317 \pm 13	163 \pm 7	266 \pm 6	161 \pm 8	264 \pm 6
	Real Pitch (μm)	49 \pm 10	37 \pm 9	81 \pm 12	76 \pm 11	85 \pm 20	83 \pm 6	145 \pm 17	128 \pm 17
	SUM (μm)	243	341	289	394	248	349	306	392
	Real Diameter (μm)	240 \pm 13	322 \pm 11	260 \pm 8	350 \pm 20	183 \pm 7	277 \pm 9	186 \pm 7	280 \pm 10
7.5 W	Real Pitch (μm)	0	23 \pm 5	43 \pm 10	37 \pm 5	63 \pm 15	63 \pm 14	103 \pm 13	95 \pm 16
	SUM (μm)	240	345	303	387	246	339	289	375

I-V tests

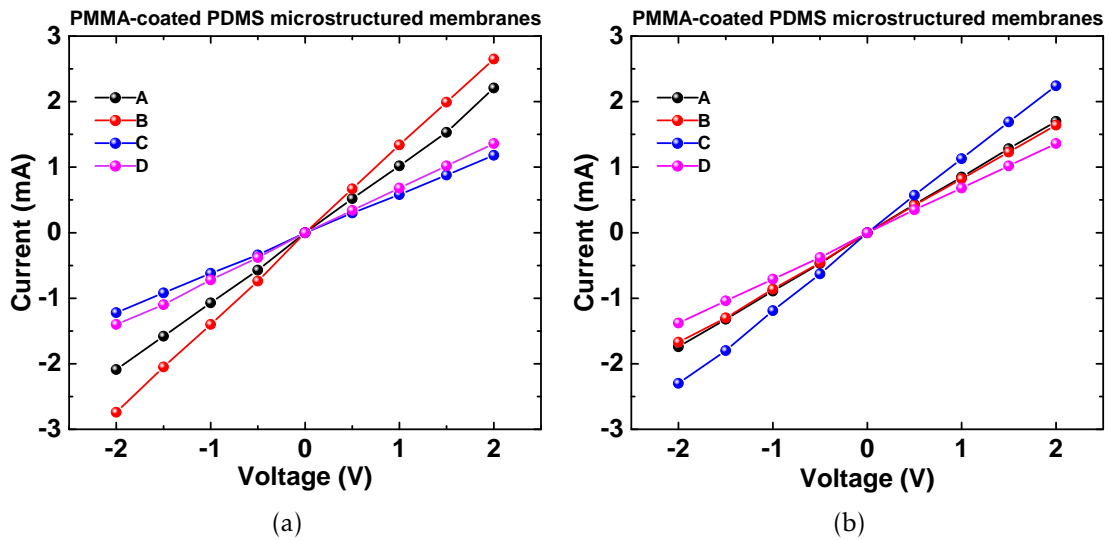


Figure B.1: Voltage sweep from -2 to 2 V proving the ohmic behaviour of four membranes produced with (a) Semi-spheres with diameter = 200 μm and pitch = 150 μm . (b) Semi-spheres with diameter = 200 μm and pitch = 200 μm .

Coated-PDMS microstructures measurements

Table C.1: Measurements of dimensions of the fabricated microstructures with carbon coating and with carbon coating with PMMA. Values presented correspond to average values \pm standard deviation of a minimum of 15 measurements.

	Carbon				Carbon + PMMA			
	Horizontal		Vertical		Horizontal		Vertical	
	150	200	150	200	150	200	150	200
	μm	μm	μm	μm	μm	μm	μm	μm
	330	368	291	296	317	372	283	275
Diameter (μm)	\pm	\pm	\pm	\pm	\pm	\pm	\pm	\pm
	10	11	25	10	13	12	11	25
		36	46	103		54	55	104
Pitch (μm)	0	\pm	\pm	\pm	0	\pm	\pm	\pm
		7	11	14		12	8	15
	110	140	110	140	104	155	104	155
Height (μm)	\pm	\pm	\pm	\pm	\pm	\pm	\pm	\pm
	16	5	16	5	8	10	8	10

Pressure applying system

Herein, the code section related to the motor motion in order to properly proceed to pressure application is shown. All the assigned variables are also shown.

```

1 // Motor Pins
2 const int stepPin = 7;
3 const int dirPin = 8;
4
5 // Lower steps
6 #define MS1 3
7 #define MS2 5
8 #define MS3 6
9
10 int steps = 1; // Steps chosen by the operator during program. Steps can go
    from 1 to 10 meaning 70 um to 700 um
11 int DT = 1000;
12 float TT = 0.05;
13 int cycles = 9999; // Cicles
14 float frequency = 0.5 ; // Frequency chosen by the operator by controlling
    the potentiometer
15
16 void funcao1(){
17
18 digitalWrite(MS1, HIGH); // Programing 1/16 step
19 digitalWrite(MS2, HIGH);
20 digitalWrite(MS3, HIGH);
21
22 int cycle1 = 0;
23
24 TT=1.0/frequency; // Period
25 DT= int(TT/(4.0*steps)*1000.0); //Delay Time DD=(Period/4*steps)*1000
26
27 while ( cycle1 < cycles){ // Program keeps running until 9999 cycles
28
29 digitalWrite(dirPin,HIGH); // Steps in one direction
30 for(int x = 0; x < steps ; x++) {
31
32 digitalWrite(stepPin,HIGH);
33 delay(DT);
34 digitalWrite(stepPin,LOW);
35 delay(DT);
36 }
37
38
39 digitalWrite(dirPin,LOW); // Steps in the other direction

```

```
40 | for(int x = 0; x < steps ; x++) {  
41 |  
42 | digitalWrite(stepPin,HIGH);  
43 | delay(DT);  
44 | digitalWrite(stepPin,LOW);  
45 | delay(DT);  
46 | }  
47 |  
48 |  
49 |  
50 | cycle1 = cycle1 + 1;  
51 | }  
52 | }
```

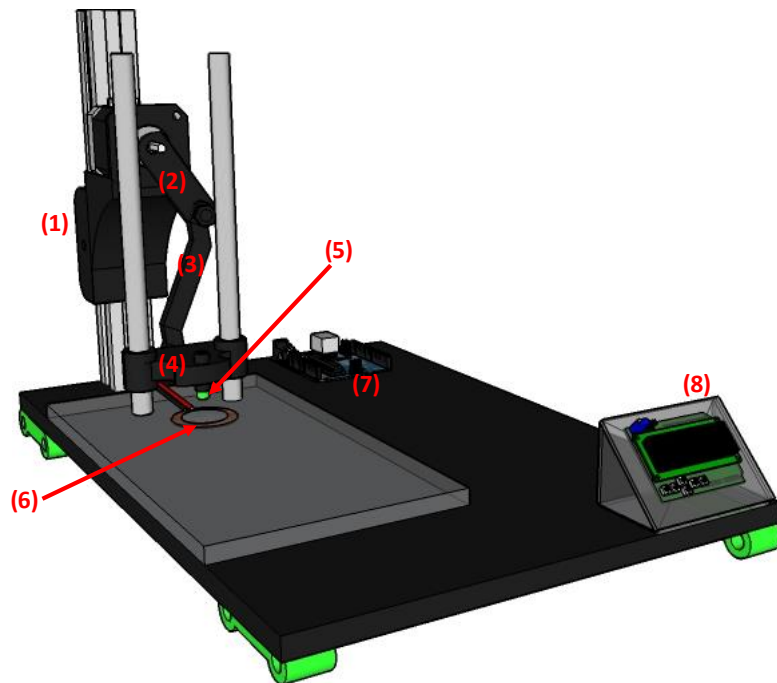


Figure D.1: Schematic representation of the developed system. (1) 3D printed stepper motor support (2) and (3) 3D printed components responsible for converting radial movement in vertical movement (4) 3D printed component that slides over two parallel bars and holds the rubber (5) Rubber that acts as the final object applying the force (6) Piezoelectric sensor capable of detecting force (7) Arduino board controlling the system (8) LCD for an easier user interface.

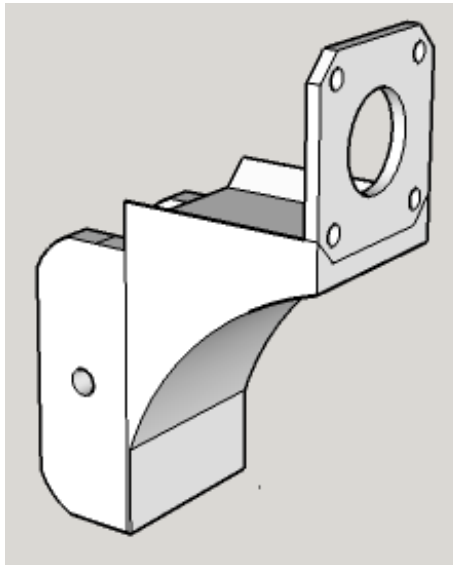


Figure D.2: Sketch in SketchUp of component 1 of the homemade system to posterior 3D printing.

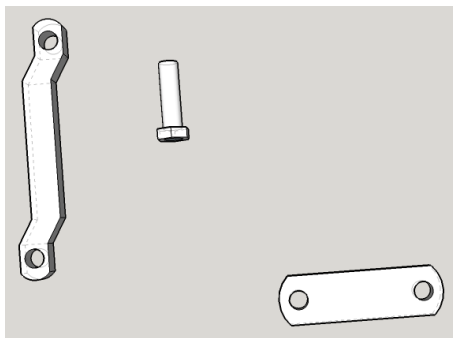


Figure D.3: Sketch in SketchUp of components 2 and 3 of the homemade system to posterior 3D printing.

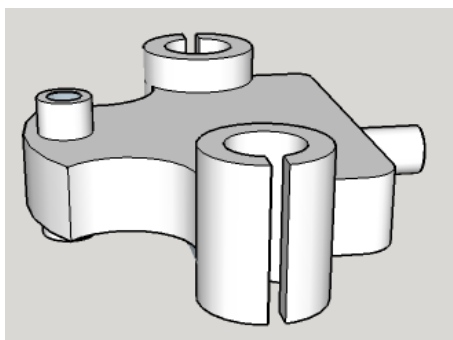


Figure D.4: Sketch in SketchUp of component 4 of the homemade system to posterior 3D printing.

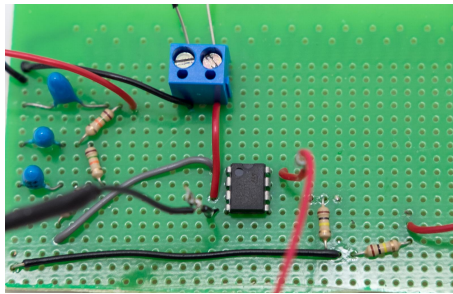


Figure D.5: RC Low-Pass Filter with Op Amp Buffer with 3 poles with a cutting frequency of 10 Hz.

Sensor operation principle

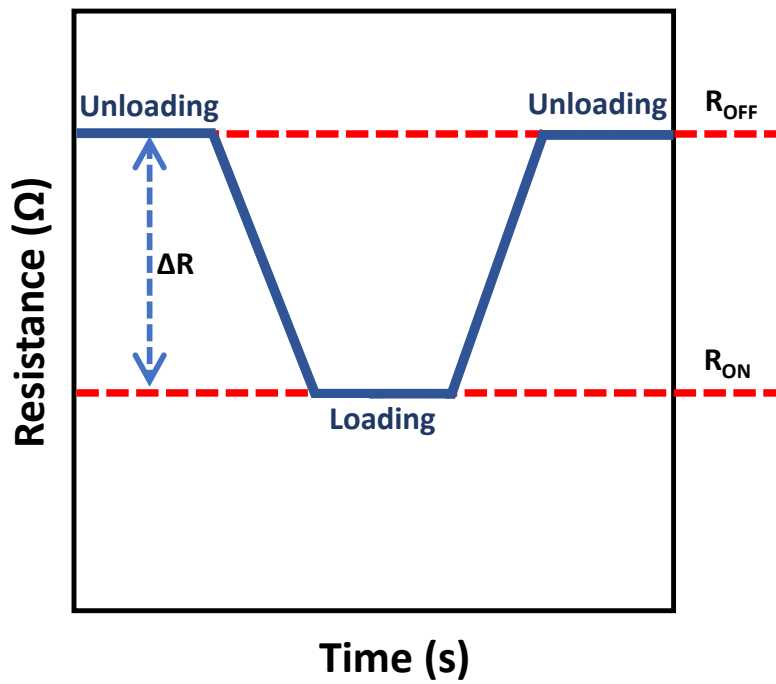


Figure E.1: Sensor operation principle based on resistance changes in responses to loading and unloading (R_{OFF} : unloading, R_{ON} : loading).

Resistance changes for different frequencies

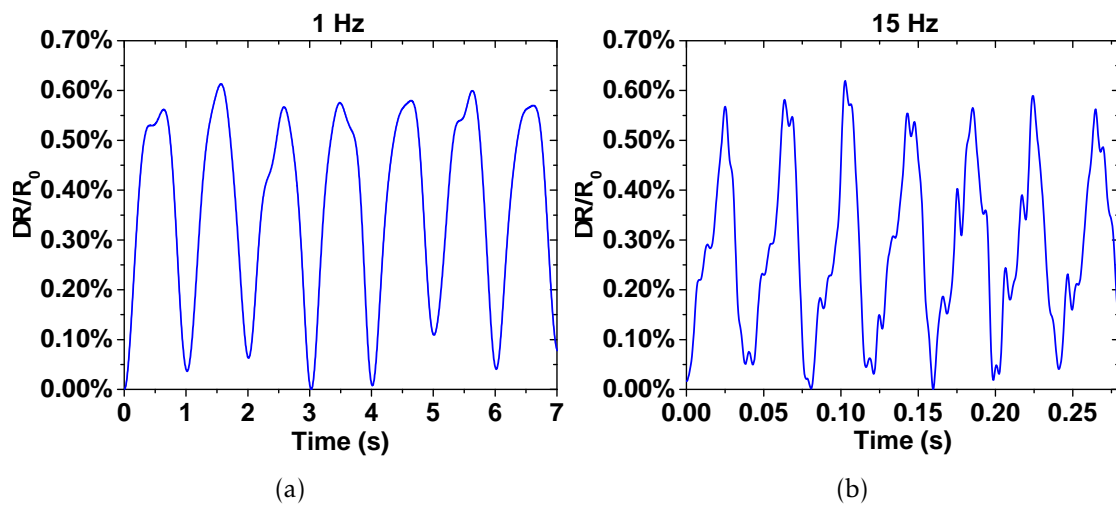


Figure F.1: Resistance changes in response to an applied pressure of PMMA-coated PDMS membranes with semi-spheres with a pitch of 200 μm with a frequency of (a) 1 Hz (b) 15 Hz.

Estimated sensor price

Table G.1: Estimated sensor price regarding materials costs

	Price (€)	Quantity (kg)	Amount used (g)	Cost (€)
PDMS	250	1.1	1.187	0.326
Carbon-ink	70.54	0.1	0.322	0.002
Silver-ink	500.80	0.1	0.456	0.023
Total				0.351